applied sciences

MDPI

Article

Extraction and Characterization of Biogenic Silica Obtained from Selected Agro-Waste in Africa

Clement Owusu Prempeh [1,2,*], Steffi Formann [1], Thomas Schliermann [1], Hossein Beidaghy Dizaji [1,3] and Michael Nelles [1,2]

[1] Department of Thermochemical Conversion, DBFZ Deutsches Biomasseforschungszentrum Gemeinnützige GmbH, Torgauer Straße 116, 04347 Leipzig, Germany; Steffi.Formann@dbfz.de (S.F.); Thomas.Schliermann@dbfz.de (T.S.); Hossein.Beidaghy@dbfz.de (H.B.D.); Michael.Nelles@dbfz.de (M.N.)
[2] Department of Agriculture and Environmental Science, University of Rostock, Justus-von-Liebig-Weg 6, 18059 Rostock, Germany
[3] Institute of Chemical Technology, Universität Leipzig, Linnéstr. 3, 04103 Leipzig, Germany
* Correspondence: Clement.OwusuPrempeh@dbfz.de; Tel.: +49-(0)341-2434-523

Featured Application: The synthesized biogenic silica can be considered in applications such as catalyst support, construction material, concrete and backing material.

Abstract: Increased amounts of available biomass residues from agricultural food production are present widely around the globe. These biomass residues can find essential applications as bioenergy feedstock and precursors to produce value-added materials. This study assessed the production of biogenic silica (SiO_2) from different biomass residues in Africa, including cornhusk, corncob, yam peelings, cassava peelings and coconut husks. Two processes were performed to synthesize the biogenic silica. First, the biomass fuels were chemically pre-treated with 1 and 5% w/v citric acid solutions. In the second stage, combustion at 600 °C for 2 h in a muffle oven was applied. The characterization of the untreated biomasses was conducted using Inductively coupled plasma—optical emission spectrometry (ICP-OES), thermal analysis (TG-DTA) and Fourier-transform infrared spectroscopy (FTIR). The resulting ashes from the combustion step were subjected to ICP, nitrogen physisorption, Energy dispersive X-ray spectroscopy (EDX) as well as X-ray diffraction (XRD). ICP results revealed that the SiO_2 content in the ashes varies between 42.2 to 81.5 wt.% db and 53.4 to 90.8 wt.% db after acidic pre-treatment with 1 and 5 w/v% acid, respectively. The relative reductions of K_2O by the citric acid in yam peel was the lowest (79 wt.% db) in comparison to 92, 97, 98 and 97 wt.% db calculated for corncob, cassava peel, coconut husk and cornhusk, respectively. XRD analysis revealed dominant crystalline phases of arcanite (K_2SO_4), sylvite (KCl) and calcite ($CaCO_3$) in ashes of the biomass fuels pre-treated with 1 w/v% citric acid due to potassium and calcium ions present. In comparison, the 5 w/v% citric acid pre-treatment produced amorphous, biogenic silica with specific surface areas of up to 91 m^2/g and pore volumes up to 0.21 cm^3/g. The examined biomass residues are common wastes from food production in Africa without competition in usage with focus application. Our studies have highlighted a significant end-value to these wastes by the extraction of high quality, amorphous silica, which can be considered in applications such as catalyst support, construction material, concrete and backing material.

Keywords: biogenic silica; African biomass fuels; thermochemical conversion; ash characterization; combustion

Citation: Prempeh, C.O.; Formann, S.; Schliermann, T.; Dizaji, H.B.; Nelles, M. Extraction and Characterization of Biogenic Silica Obtained from Selected Agro-Waste in Africa. *Appl. Sci.* **2021**, *11*, 10363. https://doi.org/10.3390/app112110363

Academic Editor: Alberto Villa

Received: 4 October 2021
Accepted: 25 October 2021
Published: 4 November 2021

1. Introduction

Lignocellulosic residues, also known as biomass, have a pivotal role in the context of sustainable development due to their unique properties. They offer biodegradability, which contributes to a healthy ecosystem, as it can drastically reduce greenhouse gas emissions compared to fossil fuels [1,2]. The combustion of biomass fuels is perceived as carbon-neutral in many perspectives as it results in no net increase of greenhouse (GHG)

emissions on a life-cycle basis. Plants are able to capture the same amount of CO_2 through photosynthesis during the different stages of plant growth. Thus, the same amount of CO_2 is released into the atmosphere from the combustion process, which is reabsorbed by the plants for photosynthesis [3]. Furthermore, since the combustion operation is performed in sufficient air atmosphere, it is assumed that the entirety of the CO released during this reaction is converted to CO_2.

In developing countries, biomass supplies most energy services, but in inefficient implementations, mainly for cooking and heating space [4]. Major negative environmental impacts of biomass reliance and usage include increased air pollution and carcinogenic health problems to users [5]. However, more resourceful biomass applications are expected in the future, such as the production of biogas and liquid fuels for cooking, value-added materials, and power generation [6]. In addition, with climate protection policies intensified by the EU [7] and AU [8] to achieve CO_2 neutrality by 2050 [9], the utilization of biomass waste is seen as a promising strategy to reduce the effects of climate change because of its potentials as a domestic and environmentally sound renewable fuel. The additional motivation that has spurred renewed interest in biomass residues, especially for developing countries, includes being part of the global industry as manufacturers of value-added materials, promising increased revenues, and job creation [10].

Against this background, numerous efforts have been undertaken to assess and characterize lignocellulosic residues of Africa origin individually [4,11–14] or as part of a composite investigation [15–19] to find an improved utilization. Dasappa [18] investigated the potential of biomass energy for electricity generation in Sub-Saharan Africa, whereas Duku et al. [4] conducted a comprehensive review of the biomass resources and biofuels potential in Ghana. In addition, Kemausuor et al. [6] assessed the biomass residues availability in Ghana and their potential in meeting the country's energy demand using crop residues. While there is a wealth of information on the material properties of a range of lignocellulosic fibres, including several studies on rice husk and rice straw, miscanthus, and sugarcane bagasse in Europe [20,21], the characterization studies of predominant and accessible residues in Africa (such as cassava, yam, coconut, corncob, and cornhusk) are still underrepresented. These foodstuffs provide over 90% of the continent's food needs and predominantly for Western and Central Africa [4]. However, extensive reviews reported in the literature so far on these biomass fuels are on their potential, and only a few are exclusively presented as a systematic study on material properties or the prospect of value-addition [22,23]. As a result, a thorough investigation is required, while also providing information on value addition processes for these residues. Such efforts are expected to result in better utilization, opening a wide range of possibilities for many developing countries.

As a case study in Ghana, Table 1 depicts the theoretical and technical potential of primary residues of Ghana in 2011 [6]. Other minor agricultural residues in Ghana include rice husk, oilseed cake, sugarcane bagasse and oil palm empty fruit bunch. The study of Kemausuor et al. [6] highlighted the vast potential regarding residues availability and shed light on the government's intervention and commitments to promote the cultivation of agricultural produce. For example, through the President's Special Initiative on cassava production, the FAO statistics reported a significant increase in production figures from 2001 to 2007 [24]. Thus, approximately 9.95 million tonnes of the crop were harvested from an area of 800,000 hectares. In addition, about 1.10 million tonnes of maize were harvested from 750,000 hectares within the same production year [3]. Jekayinfa et al. [16] estimated the residue to product ratio values of cassava peelings, corncob, and corn husk at 0.25, 0.27 and 0.20 g/g, and residue amount at 9.54, 1.30 and 0.96 metric tonnes (Mt), respectively. These values show a huge biomass residue potential with minimal end-use due to the lack of study or available options for value addition.

Table 1. Potential of crop residues in Ghana.

Crop	Theoretical Potential of Residue (Mt/Year)	Technical Potential of Residue (Mt/Year)
Cassava peeling [P]	3.6	0.72
Yam straw [F]	3.2	2.5
Coconut husk [P]	0.12	0.12
Corncob [P]	0.49	0.49
Corn husk [P]	0.34	0.34

[F] denotes a field-based residue, whereas [P] indicates a processing residue. Modified from Kemausuor et al. [6] with permission from Elsevier, Copyright (2014).

Silicon dioxide (silica) is one of the most valuable inorganic materials with a range of industrial applications such as an alternative to ordinary Portland cement [25], a precursor for the synthesis of water glass [26], a rubber filler [27], an adsorbent for the treatment of effluents [28], silica mesoporous material [29], a support system in catalysis operations [30] and coatings in epoxy paints [31]. However, the conventional synthesis of silica from a mineral-based precursor, tetraethyl orthosilicate (TEOS), involves a high thermal hydrolysis process. This process is energy-consuming and cost-intensive. In addition, secondary products (CO_2 and voluminous amount of wastewater) that are environmentally unfriendly are generated [32–35]. Therefore, these downsides along the silica production route have hindered their wide applications.

Over the last decades, there have been renewed interest in silica extraction from naturally occurring silica plants, including rice husk and straw, wheat straw and cereal remnant, oat husk and spelt husk [36–39]. Si-accumulating plants present a viable alternative that can be harnessed for producing silicon-based materials [35–41]. Vaibhav et al. [42] investigated the use of agricultural wastes to produce silica nanoparticles. Through thermochemical conversion and leaching procedures, pure silica can be generated from the residues as the bottom ash [43] or fly ash [44] contains a significant amount of silica. The high silica content in fly and bottom ashes can find applications in the production of zeolites and admixtures in cement [25,44].

Lignocellulosic biomass constitutes cellulose, hemicellulose, and lignin [45] with considerable amounts of alkali and alkaline earth metallic species (AAEMs), such as sodium, potassium, calcium, magnesium, and iron, etc. [46]. The high presence of AAEMs can influence the physiochemical properties of the resulting biogenic silica during combustion, and thus, needs to be removed from the organic matrix before thermal treatment [47]. The use of organic acid such as citric acid to remove the content of AAEMs from the biomass is recommended over inorganic acids due to environmental considerations [48]. The effectiveness of carboxylic acid in producing high-purity amorphous silica from rice husk has been reported by Umeda et al. [49]. More importantly, for high-end applications such as catalyst support, the generated biogenic silica must attain specific purity, crystallinity, and porosity [50]. So far, the use of agricultural waste products is economically and commercially successful in many applications. Utsev et al. [51] investigated coconut shell ash as a partial substitute of ordinary portland cement in concrete production. Other efforts have been made to understand the role of major constituents of coconut fibres and yam peels in the absorption of ionic dyes [52] and removal of Cd(II) ions from an aqueous solution [53], respectively. Interestingly, limited studies (Adepoju et al. [15], Biswas et al. [38], Utsev et al. [51] and Anuar et al. [54]) have been conducted on residues from cassava, yam, coconut, corncob, and cornhusk as potential silica sources.

Therefore, this study critically examines some primary biomass resources accessible in Africa and presents a systematic characterization of their chemical compositions, morphological and thermal behaviour, aspects of textural properties and X-ray diffraction in respect of the five lignocellulosic residues. Hence, the characteristics of silica derived from these residues as a new possible alternative source for silica-based materials are investigated. With the continent's agricultural potential and considering the voluminous quantity

of wastes generated, these agricultural residues can be converted into the fabrication of valuable resources. Therefore, it is envisaged that such efforts will lead to better usage of crop residues, opening a new and wide array of options for many developing countries while tackling the challenges associated with waste management in Africa.

2. Materials and Methods

2.1. Material Used and Sample Preparation

Biomass fuels/residues of cornhusk, corncob (*Zea mays*), yam peelings (*Dioscorea spec.*), cassava peelings (*Manihot esculenta*) and coconut shell (*Cocos nucifera*) were obtained from farmers in the Ashanti region, Ghana. Upon collection, they were washed in tap water to remove adhered soil particles and dried in an air oven at 105 °C. The biomass fuels were cut into smaller particles (<1 mm) using the hammer mill (Netzsch-Condux, Hanau, Germany) and then stored in airtight plastic containers until further use.

Using 3000 mL of tap water and 150 g of the solid residues, a solid-(dry mass) to-liquid ratio of 1:20 (g/mL), the biomass fuels were leached in tap water dissolved in 1 or 5 wt.% citric acid (CA) (Sigma-Aldrich, Steinheim, Germany, purity of >99.99%) at 50 °C for 2 h. The leaching conditions follow the experimental protocol of Schliermann et al. [55], and this allowed the comparison of the behaviour of the resulting ashes (biogenic silica powders) regarding purity and textural properties at different citric acid concentrations. The leached samples were rinsed with tap water and dried overnight at 105 °C.

For the combustion process, weighed amount of the untreated and acid-leached biomass fuels were combusted at 600 °C in a lab-scale muffle furnace (Nabertherm 1185H66EA, Lilienthal, Germany) under air atmosphere for 2 h at a heating rate of 6 °C/min. The resulting ashes were then cooled to room temperature in the furnace. The combustion temperature was chosen based on literature data [14].

The biomass fuels were abbreviated as CasP, YamP, CocH, CorC, and CorH to represent cassava peelings, yam peelings, coconut husks, corncobs, and cornhusks, respectively. Furthermore, the resulting ashes of the biomass fuels were identified as X-U-A-Y, where X is the name of the biomass fuels, U is untreated, A represents the ashes, and Y is the acid concentration used for leaching (1 and 5 *w*/*v*%). Figure 1 illustrates the sample preparation and the extraction process to prepare the silica-rich ashes.

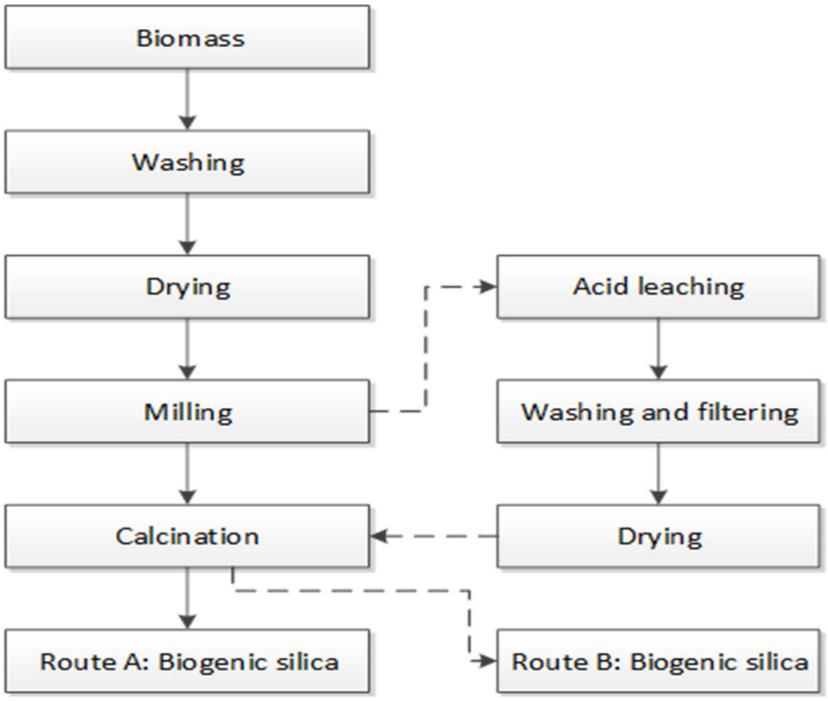

Figure 1. Extraction of biogenic silica from agricultural biomass residues to produce silica-rich ash.

2.2. Analysis of Physical and Chemical Properties

To fully characterize the biomass fuels, elemental analysis of the raw, leached biomass fuels and the generated ashes were carried out by inductively coupled plasma-optical emission spectroscopy (ICP-OES) according to the DIN EN ISO 16967;2015-07, DIN EN ISO 1. ICP-OES analysis provided information on the distribution of fundamental organic elements and ash forming elements embedded in the raw and leached biomass fuels.

FTIR analysis of the biomass fuels and the ashes from the combustion was performed using an FTIR-spectrometer (PerkinElmer, Solingen, Germany) to identify the main organic compounds and various functional groups within the ashes and raw biomass fuels. The spectrum scope was in the range of 400–4000 cm^{-1} with a resolution factor of 1 cm^{-1}.

The phases in the resulting ashes were determined by X-ray diffraction (XRD) apparatus (Malvern Panalytical GmbH, Kassel, Germany) equipped with Ni-filtered, Cu-Kα radiation (λ = 1.54 Å). The chemical composition spectrum of the ash samples was calculated using the Energy-dispersive X-ray fluorescence spectroscopy (EDX) (Bruker, Massachusetts, USA).

The textural properties of the ashes were determined using autosorb iQ-MP/XR apparatus, Quantachrome, USA. The samples (~0.1–0.3 g) were degassed by heating at 250 °C under vacuum (ca. 0.4 kpa) for 10 h to remove non-dissociative, physically adsorbed water molecules from the sample surface and within the pores. The Brunauer, Emmett and Teller (BET) surface area was determined by fitting the adsorption data to the BET equation in the relative pressure range of (p/p_0) = 0.05–0.3. Nitrogen was used as the adsorptive gas at 77 K, with a standard value of 0.162 nm^2 for the molecular cross-section of nitrogen. The total pore volume was obtained at a relative pressure (p/p_0) = 0.98. The pore characteristics were calculated using indirect molecular adsorption methods such as nonlocal density functional theory (NLDFT).

Canon EOS 250D (Canon Ltd., Krefeld, Germany) was used to capture the visual appearances of the ashes after the combustion process. All the images were recorded at the same time under natural light with no flashing light.

2.3. Thermal Analysis of Biomass Fuels

To assess the rate of thermal degradation of the biomass fuels, the weight loss caused by changing temperature was measured according to the experimental method of Hilbers et al. [56]. The thermal degradations were carried out in a simultaneous thermal analysis (STA 449 F3 Jupiter®, NETZSCH, Selb, Germany) in a synthetic air flow atmosphere with a 100 mL/min flow rate under a heating rate of 10 K/min. Approximately 10–20 mg of biomass fuels were placed in alumina crucibles and the samples were heated from room temperature to 600 °C. To create homogenous starting material for the STA analysis, each biomass fuel was ground to a particle size of less than 0.5 mm with a cutting mill (IKATM MF 10 basic Mikrofeinmühle) and vigorously mixed in a plastic box. The TG and DTG curves were recorded simultaneously along the temperature increase.

3. Results and Discussion

3.1. Solid Fuel Analysis

Table 2 presents the fuel analysis results, including proximate and ultimate analysis, the lower heating value of the biomass fuels, and the chemical composition of the fuel ash. According to Table 2, all the untreated biomass fuels are characterized by an ash content (AC) of 1.85–5.04 wt.% db. The moisture content (MC) of all tested samples is in the range of approximately 2.71–10.7 wt.% wb. The fuel ash analysis results show predominant ash forming elements being compounds of K, Ca, Al, Mg, Na, P, S, and Si. The K concentration was high in the untreated biomass fuels but reduced significantly along with other impurities after the chemical pre-treatment. Observed silica content in the untreated and chemically pre-treated biomass fuel ash increased from 11.53–44.13 to 38.62–70.74 wt.% db, respectively. Similar silica enrichment after acidic pre-treatment of biomass fuels has been reported elsewhere [35,36]. The high carbon and oxygen contents of 44.4–50.10 wt.% db suggest the presence of oxygen-containing functional groups on the

biomass fuels' surface and the lignocellulosic nature of samples [57]. The lower heating values (LHV) define the amount of heat released during the combustion ranged between 16.36–18.8 MJ/kg db as indicated in Table 2.

Table 2. Fuel and fuel ash properties of untreated (U) and acid leached (L), cassava (CasP), yam (YamP), coconut (CocH), corncob (CorC) and corn husk (CorH). Inorganic species are specified on fuel ash basis. Abbreviations wb, db, and n.d. stand for wet basis, dry basis and not detected. Oxygen is calculated by difference. VM: volatile matter; AC: ash content; MC: moisture content; and LHV: lower heating value.

		CasP		YamP		CocH		CorC		CorH	
Parameter	**Unit**	**U**	**L**	**U**	**L**	**U**	**L**	**U**	**L**	**U**	**L**
VM	wt.% db	77.1	79.7	79	82.4	68.6	79.2	79.9	86.6	82	87.4
AC	wt.% db	5.5	3.59	4.57	2.38	5.04	0.93	2.32	0.74	1.85	1.04
MC	wt.% wb	9.96	4.23	13.6	2.71	10.7	1.73	5.34	3.53	9.9	5.18
LHV	MJ/kg db	16.52	17.3	16.36	16.64	18.12	18.8	17.49	17.68	17.14	17.41
C	wt.% db	45	47.3	44.4	45.3	49.3	50.1	47.7	47.6	47.4	46.6
H	wt.% db	5.76	5.93	5.82	6.23	5.24	5.92	5.91	5.86	5.87	5.81
N	wt.% db	1.09	1.04	1.01	1.02	0.54	0.4	0.66	0.58	0.26	0.23
O	wt.% db	49.12	46.77	49.69	48.37	45.36	43.98	46.39	46.54	46.73	47.59
S	wt.% db	0.12	n.d	0.09	0.1	0.1	n.d	n.d	n.d	n.d	n.d
					Fuel ash analysis						
Al_2O_3	wt.% db	5.67	8.46	1.76	2.87	0.84	1.57	0.51	0.79	1.00	0.68
CaO	wt.% db	14.80	30.31	3.91	8.07	4.96	16.76	2.23	9.82	6.65	10.69
Fe_2O_3	wt.% db	2.23	3.03	0.65	2.11	0.92	2.07	0.87	2.98	0.02	0.84
K_2O	wt.% db	40.84	1.83	46.66	17.67	61.98	4.24	62.44	8.21	33.60	1.61
MgO	wt.% db	3.96	2.62	2.22	1.97	4.67	3.07	2.97	2.49	0.00	2.67
MnO	wt.% db	0.14	0.08	0.08	0.12	0.06	0.04	0.10	0.05	8.50	0.05
Na_2O	wt.% db	0.36	1.10	0.43	1.04	4.45	2.96	0.09	2.23	0.18	1.72
P_2O_5	wt.% db	4.35	2.94	11.15	8.88	4.48	5.81	3.98	4.64	0.02	1.16
SiO_2	wt.% db	20.01	38.62	26.70	45.22	11.53	44.57	20.82	49.53	44.13	70.74
SO_3	wt.% db	6.82	9.68	5.98	11.23	5.86	18.17	5.67	18.52	5.27	9.37
Others *	wt.% db	0.82	1.33	0.45	0.82	0.25	0.74	0.31	0.75	0.61	0.47

"Others *" include trace minerals such as BaO, Cr_2O_3, CuO, Li_2O, NiO, SrO, TiO_2, ZnO.

3.2. TGA Analysis of Biomass Fuels

According to Ma et al. [58], TGA is a useful tool to examine the mass-loss characteristics and kinetics parameters of the thermal breakdown process. The results of the TGA and DTG analysis during the combustion process of the biomass fuels are shown in Figure 2. The combustion process occurred in three stages: 68–281 °C, 307–381 °C and 408–454 °C. The first two stages were characterized by rapid devolatilization. A considerable amount of the sample's weight was lost (25.43–45.15 wt.% db), with two distinct mass-loss peaks indicated in the DTG curves. Conversely, the third stage depicted a slow degradation process.

In the first phase of the first stage (25–105 °C), there was a small percentage of mass loss (3.13–5.75 wt.% db), which corresponds to water evaporation in the samples [58]. The second phase of the first stage, where the maximum decomposition rate occurred, is mainly attributed to the decomposition of hemicellulose. Since hemicellulose is a mixture of several polymerized monosaccharides (xylose, mannose, glucose, galactose, and arabinose, among others) with a lower degree of polymerization, its thermal stability is lower than that of cellulose [58–60], and this occurred at a temperature between 268.1 to 281.3 °C. Ma et al. [58] reported that the predominant temperature for hemicellulose breakdown appears between 139–323 °C for palm kernel shell, whereas Dhyani et al. [61] reported the decomposition temperature for hemicellulose in the range of 220–315 °C.

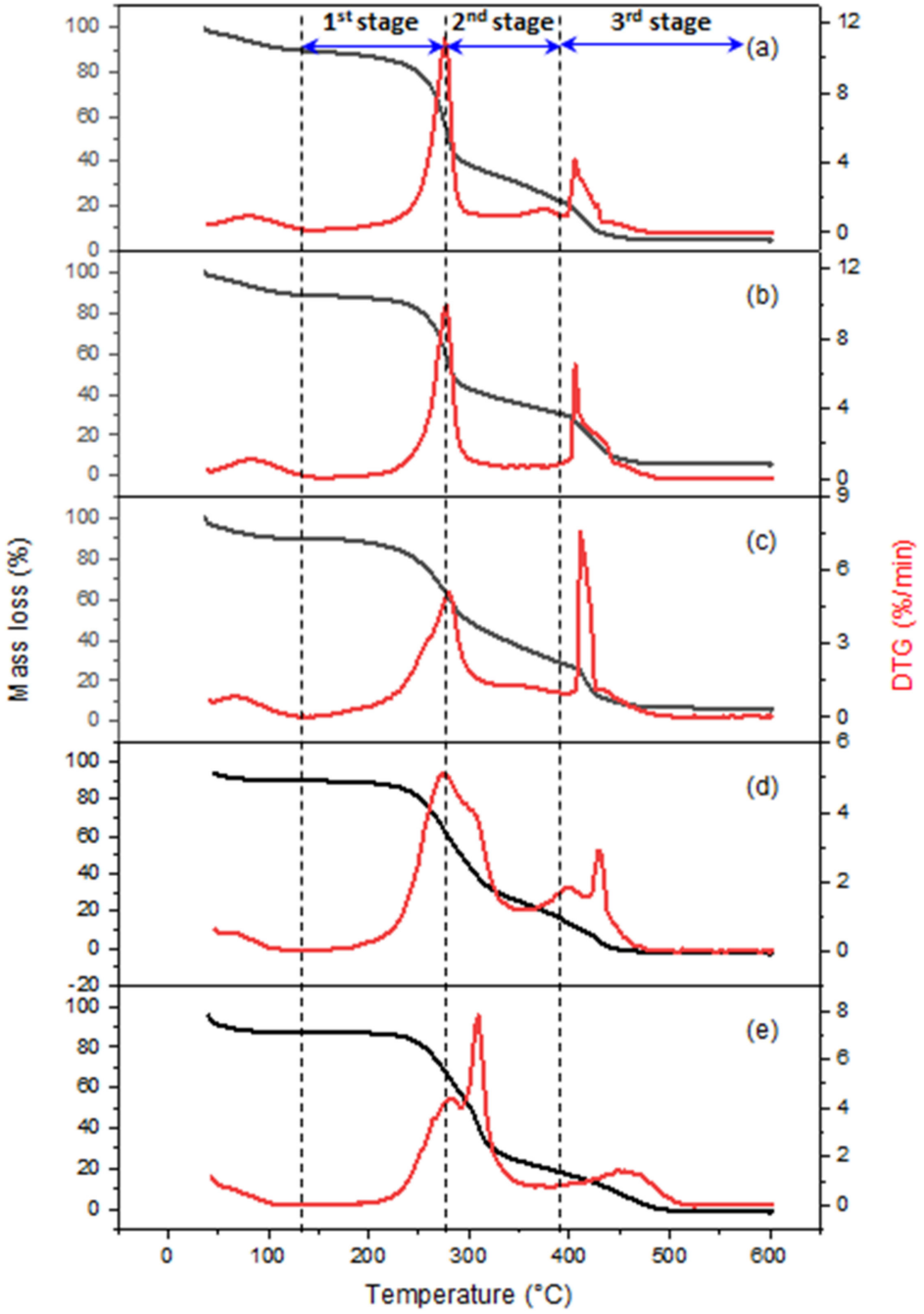

Figure 2. TG (black curve and y-axis on the left side) and DTG (red curve and y-axis on the right side) profiles of untreated residues of (**a**) cassava, (**b**) yam, (**c**) coconut, (**d**) corncob, and (**e**) cornhusk.

In the second stage (307–381 °C), a simultaneous degradation process was observed, owing primarily to the presence of cellulose [58], which accounts for approximately 20.25–30.69 wt.% db of mass loss. In yam and coconut biofuels, the second devolatilization stage (i.e., decomposition of cellulose) was not observed. The decomposition of the organic compounds occurred in parallel, in a super-compositional manner, as shown in the DTG curves. However, cellulose decomposition was observed in cassava, corncob, and cornhusk with the maximum decomposition rate at a temperature between 307–381 °C. Because cellulose is a high-molecular-weight substance with a long linear chain formed of D-glucosyl groups [62], and a portion of cellulose has a crystal structure composed of organized microfibrils, it degrades more slowly than hemicellulose [63].

The third stage only accounts for a minor portion of mass loss (6.14–7.81 wt.% db) with a maximum decomposition rate at a temperature range of 408.3–454.7 °C. This stage might be attributed to the degradation of lignin, which is the most stable component of lignocellulosic biomass. It is difficult to decompose and requires higher decomposition temperatures, as the decomposition occurs slowly along the whole combustion temperature range [61]. From Figure 2, the distinct weight loss peaks in the DTG curves of cassava, yam and coconut were considerably different from corncob and cornhusk, which presented only one distinct peak and an additional "shoulder" peak. This could be a result of a low lignin content compared to the residues of cassava, yam and coconut. Lignin is an amorphous substrate that resides in the minute spaces between cellulose microfibrils. It is covalently bonded to hemicellulose and crosslinked to polysaccharides and contributes to the crystallinity of biomass fuels [58–60]. It is conceivable that there is a higher lignin content in cassava, yam, and coconut. Thus, they were thermally degraded more slowly than the other biomass residues, corncob and cornhusk, resulting in distinct mass losses of hemicellulose and cellulose [64]. Ceylan et al. [65] observed a similar result of two discrete mass-loss maxima in hazelnut husk with a high lignin concentration (39%). Similar observations for other biomasses that showed only one distinct peak in the DTG curve (such as pinewood [66], bamboo [67] and corn stover [68] or with a minor "shoulder" (e.g., wheat straw [68]) have been reported in the literature. In addition, charring of the biomass fuels has been reported to occur at this stage due to lignin breakdown [69,70].

Therefore, it can be concluded that the overall decomposition behaviour of cassava, yam, coconut, corncob, and cornhusk is due to the decomposition of the primary organic materials: cellulose, hemicellulose, and lignin, with the extent of complexity of the TGA curves depending on the definite compositions of the individual components of the lignocellulosic biomasses [61]. Similar decomposition behaviours of cellulose, hemicellulose and lignin have been reported in the study of Yang et al. [60]. They noted that the degradation of hemicellulose and cellulose showed the highest mass loss rate at 268 °C and 355 °C, respectively, and lignin was the most difficult of the three to disintegrate [60,61]. According to Mansaray et al. [71], the hemicellulose and cellulose constituents are the primary contributors to the evolution of volatile compounds, whereas the degradation of lignin leaves behind char particles as the direct product.

3.3. FTIR Analysis

The evolution of the functional groups during the combustion of the raw biomass fuels and the ashes produced at 600 °C was examined by employing a Fourier Transformation Infrared (FTIR) analysis. The characteristic peaks and functional groups are presented in Figure 3 and Table 3, respectively. According to the FTIR analysis, the major volatile components change in the spectra relates to the vibration generated by the O–H bonds (3000–3600 cm^{-1}), C−H groups (2900–3000 cm^{-1}), stretching vibration of C=C and C−O. These bands generally disappear during combustion as the significant share of organic compounds (i.e., cellulose, hemicellulose, and lignin) is decomposed as observed in in Figure 3 (bottom). The bands at approximately 1065, 972, and 1415 cm^{-1} are corresponding to the stretching vibration of CO_3^{2-}, which corresponds to the content of calcite ($CaCO_3$) in the ashes. The positions of the bands agree with the reference calcite in Figure 3 (bottom). Beidaghy Dizaji et al. [50] also detected the formation of $CaCO_3$ in the silica-rich ashes obtained from rice husk and rice straw using a diffractometry technique (i.e., quantitative Rietveld refinement of XRD data). They reported that the formation of this phase could result from a reaction between CaO in the ash and the ambient CO and CO_2 gaseous species after the combustion. It is probably because some of the ashes were regularly exposed to the ambient air for different analyses after production considering their production time. The infrared spectra at the ranges 400–600, 778–799, and 1035–1125 cm^{-1} could be attributed to bending, stretching, and asymmetrical stretching vibration of Si–O–Si, which are in line with the literature reports and the detected bands (i.e., 797 and 1065 cm^{-1}) in the reference silica sample (CWK Köstropur® 021012). Typically, the asymmetrical stretching

vibration of Si–O–Si in the wavenumber region 1035–1125 cm^{-1} obscures with several different bands such as the SO_4^{2-} bands in the region 1138–1155 cm^{-1}, R–OH groups in 1051 cm^{-1}, stretching band of aliphatic ether C–O and alcohol C–O in cellulose and hemicellulose in 1050 cm^{-1}, β-(1–4) glycosidic bonds in cellulose such as C–O–C stretching and pyranose ring skeleton vibration in the region 1159–1108 and 1027–1051 cm^{-1} [72–76].

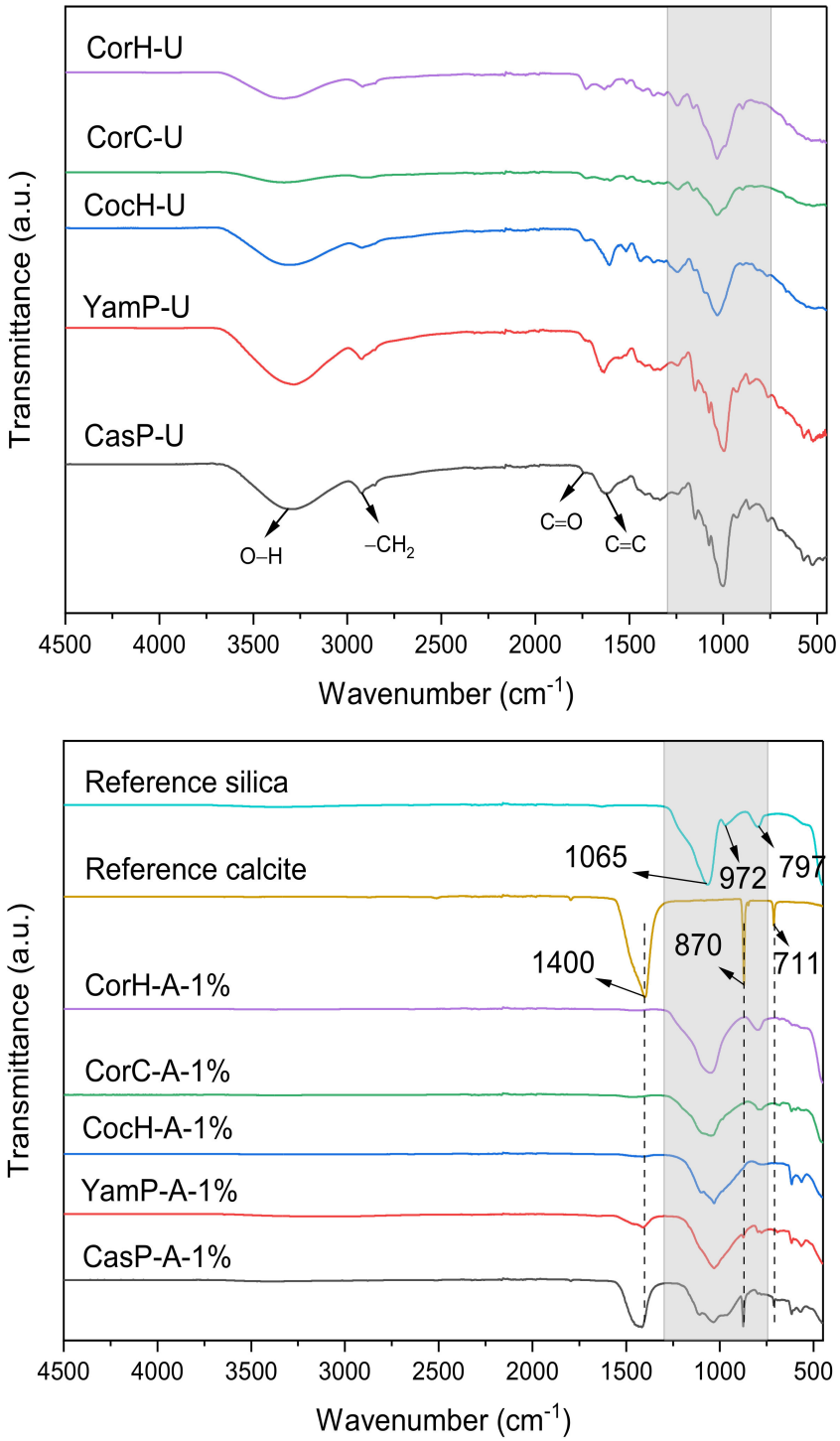

Figure 3. The evolution of the main functional groups in raw biomass (**upper**) and ashes of 1 *w*/*v*% biomass fuels (**bottom**). Ashes were generated at 600 °C and compared with the FTIR of commercial calcite and silica powders.

Table 3. The main functional groups of the three main components of the biomass fuels and the ashes produced at 600 °C during combustion characterized by FTIR.

Wavenumber (cm^{-1})	Functional Groups	Compounds	Reported Values (cm^{-1})	References
3600–3000	O-H stretching	Acid, methanol	3600–3000	Yang et al. [60]
2900–3000	C-H stretching	Alkyl, aliphatic, aromatic	2860–2970	Yang et al. [60]
1402–1415	OH bending, CO_3^{2-}, CH bending	Acid and $CaCO_3$	1440–1400, 1400–1460, 1417–1425	Magdziarz et al. [77] Nieves et al. [78] Ceylan et al. [65] Yang et al. [60]
1159–1108; 1027–1051	C–O–C stretching vibration	Pyranose ring skeletal	1170, 1082	Yang et al. [60]
1035–1125	C–O stretching, C–O deformation, OH association and Si–O–Si	C–OH (ethanol), SO_4^{2-} and SiO_2	1035–1065, 1108	Nana et al. [79] Ma et al. [80] Nieves et al. [78] Yang et al. [60]
956–972	Si–O–Si	SiO_2	956–972	Bathla et al. [81] Morrow et al. [82] Mohanraj et al. [83]
	C–H and stretching vibration of CO_3^{2-}	Aromatic hydrogen and $CaCO_3$	700–900	Ennaciri et al. [84] Bonfim et al. [26] Medina et al. [85] Liou et al. [86]
778–799	Si–O–Si	SiO_2	796, 798	Frías et al. [87]
711	Stretching vibration of C–O	$CaCO_3$	713, 709	Leng et al. [88] Ennaciri et al. [84]
400–600	C–C stretching	Aromatic hydrogen	700–400	Yang et al., 2007 [60]

3.4. Ash Analysis

Impact of the Pre-Treatment Process on the Chemical Composition of the Inorganic Fraction of Biomass Fuels

The changes in elemental composition upon treatments (1 and 5 w/v% citric acid (CA)) of the biomass fuels are shown in Figure 4. The results indicated that in untreated ash samples, the share of oxides of silica, potassium, sodium and calcium are in higher proportion compared to other ash forming elements (such as Al_2O_3, CaO, K_2O, MnO, etc.). Acidification of the biomass fuels proved to be effective in removing the above metals to substantially lower levels, as the main component of the samples was SiO_2. The reduction in the metal impurities after the pre-treatment process could be attributed to the dissolution of weakly and strongly bonded metals within the organic matrix of the biomass fuels [89], and the volatilization of metals that occurred during the thermal decomposition process [90]. Nevertheless, the ashes of some of the samples contained a considerable amount of potassium and oxides of Al constituents relative to silica even after the acidic pre-treatment. These observed effects align with similar observations made by Alyosef et al. [89] during their investigations on Egyptian diatomite.

According to the analyses, the removal efficiency of K_2O by the citric acid in yam peel was the lowest (79 wt.% db) in comparison to 92, 97, 98 and 97 wt.% db calculated for corncob, cassava peel, coconut husk and cornhusk, respectively. Chen et al. [91] have reported a K_2O removal in the proximity of 98 wt.% db after acetic acid pre-treatment of rice husk. According to Dunlop [92], hydrolysis of cellulose and hemicellulose to produce monosaccharides occurs during the leaching of biomass fuels. Consequently, the monosaccharides were assumed to block access of the leaching agent to the inorganic impurities [92]. Thus, the volatilization of K^+ ions is hindered due to their attachment to the organic matrix at temperatures below 400 °C [93].

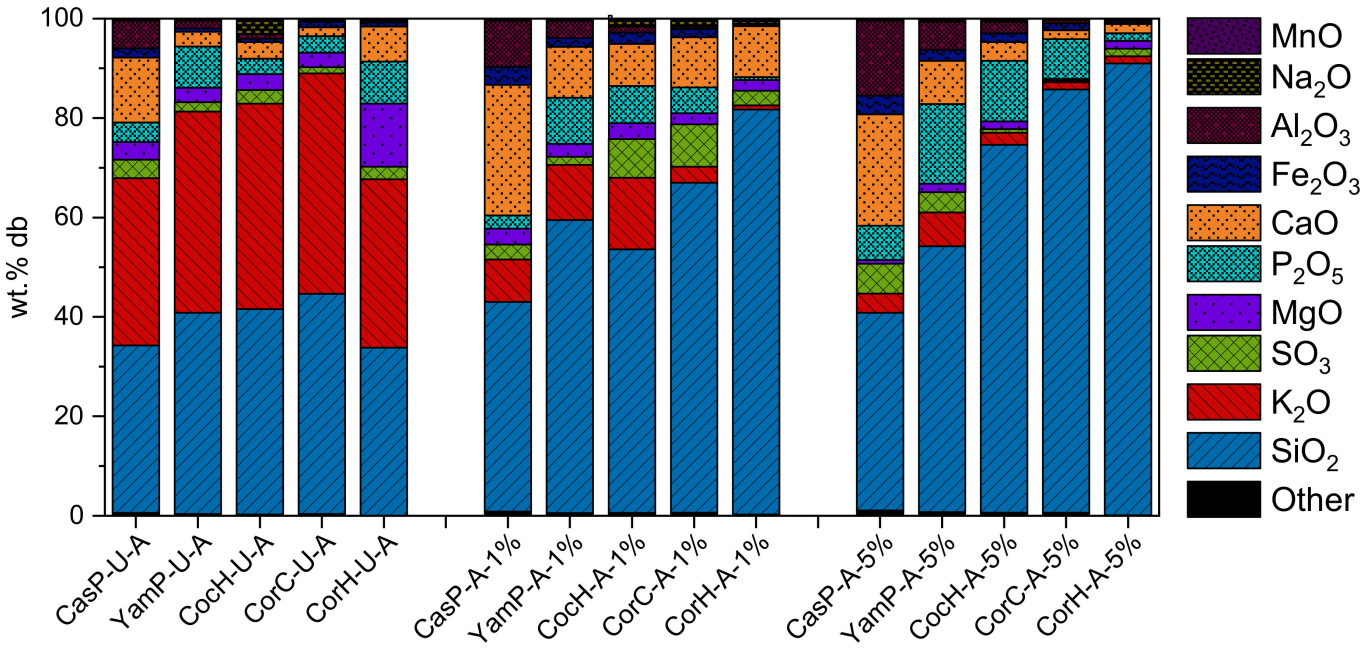

Figure 4. Chemical composition of the inorganic fraction (=100 wt.% db) of ashes obtained from the thermal treatment of the untreated and acid-leached samples with citric acid.

In this study, further removal of metals from the biomass fuels occurred in diminutive amounts with increasing concentration of the citric acid (5 w/v%). Nonetheless, the amounts of some metallic oxide (such as Al_2O_3) in 5 w/v% CA treated ashes of yam and cassava residues were more than those of 1 w/v% citric acid samples. This confirmed that the treatment of yam and cassava biomass fuels with citric acid for silica extraction or removal of Al_2O_3 might not be suitable at higher citric acid concentrations. Probably, the use of inorganic acids including HCl and HNO_3 or inorganic bases such as NH_4OH and NaOH as adopted by several researchers (Hunt et al. [94]; Amick [95]; Umeda et al. [96]) could be used in pre-treating cassava and yam biofuels. Adepoju et al. [15] reported a 61.5% silica yield from cassava periderm after leaching with HCl.

This study found higher silica content in the ashes of the acid-treated biomass fuels compared to the other ash-forming elements such as K^+ ions. The silica contents of all the studied samples under each pre-treatment (1 and 5 w/v% citric acid) increased in the following order: CorH-A-5% (90.87 wt.% db) > CorC-A-5% (85.12 wt.% db) > CorH-A-1% (81.45) wt.% db) > CocH-A-5% (73.97 wt.% db) > CorC-A-1% (66.13 wt.% db) > YamP-A-1% (58.94 wt.% db) > YamP-A-5% (53.47 wt.% db) > CasP-A-1% (42.15 wt.% db) > CasP-A-5% (39.72 wt.% db). The observed variability of silica contents across the ashes of the various biomass fuels might be due to the diverse Si-accumulation mechanism used by plants [40]. The role of silica in plants is to offer some protection against certain biotic and abiotic stressors [41]. As a result, depending on their requirements and the quantity of silica in the soil, various plants uptake varying concentrations of silica particles in the form of silicic acid [$Si(OH)_4$] from the soil [97].

Ma et al. [98] reported that the SiO_2 concentrations in plants vary owing to unequal silica deposition in tissues, variations in origin and growth circumstances (soil, humidity, sun exposure), and genotypic variations. On a dry weight basis, the silica in plant shoots can naturally fluctuate between 0.1 and 10% dry weight depending on the plant species [98,99]. In rice (*O. sativa*), cultivars usually showed a reduced silica concentration than japonica cultivars [98]. Alyosef et al. [100] found above 7 wt.% db deviation in the silica concentration of various batches of raw rice husk from different regions in Egypt. In addition, 5 wt.% db SiO_2 variations have been reported in the results of rice husk ash in India [101]. According to Ma et al. [102] and Takahashi et al. [103], silica is less deposited in most *Angiosperme*, *Gymnospermae*, *Filicopsidae*, and *Pteridophyta*. However, some plants,

such as rice (*Oryza sativa*) and sugarcane (*Saccharum officinarum*), may accumulate as much as 39 mg [104] and 10.2 mg [105] of silica per gram, respectively. Thus, the affinity for silica by the plants may influence the total concentration stored inside their shoots and roots [97], which might explain the differences in silica contents as observed in the case of *Zea mays* examined in this study. Two different parts of the plant (cob and husk) were examined, explaining the variability in silica contents. For the rest of the examined biomass fuels, the variability in silica contents may be due to differences in origin or genotypic differences, as explained above.

The variations of carbon content (not directly determined but indirectly estimated from the LOI values of the ashes) decreased from 7.8, 5.83, 4.67, 53 and 34.47 wt.% db in the untreated ashes of cassava, yam, coconut, corncob, and cornhusk, respectively to undetectable levels in the ashes of the 5 wt.% acid-leached biomass fuels.

3.5. Comparative Study of Physical Morphology, Textural Properties, and Phase Analysis of Ashes

3.5.1. Physical Morphology of Ashes from Untreated and Acid-Treated Biomass Fuels

Figure 5 shows the effects of the pre-treatment step on the physical appearance of the ashes of the untreated and the acid-leached biomass fuels. The results indicated that white biogenic silica could be generated by pre-treating the biomass in a hot citric acid solution. According to Alyosef et al. [99] and Beidaghy Dizaji et al. [36], the colouration of the ashes is an indication of completeness of a combustion process and low concentration of remaining impurities. The metallic oxides in the untreated biomass fuels result in the formation of black particles in the ashes [106]. Furthermore, the impurities increase the risk of slag formation and their role during the combustion of silica-rich biomasses have been discussed in the literature [50,107].

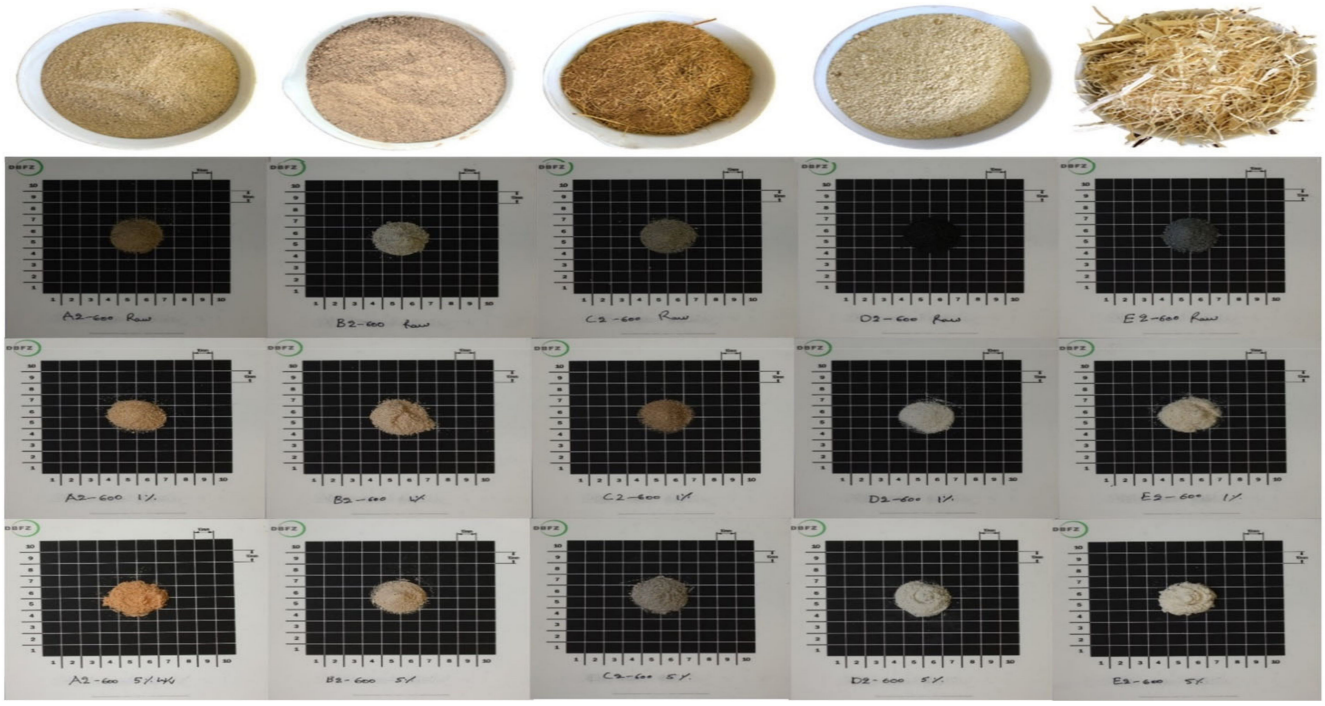

Figure 5. Visual appearances of thermally produced ashes of the raw and the acid-leached biomass fuels at 600 °C. **First row from the top**: untreated biomass fuels; **second row**: ashes of untreated biomass fuels; **third row**: ashes of 1 w/v% biomass fuels, and; **last row**: ashes of 5 w/v% biomass fuels. From left to right, biomass fuels and ashes of cassava peelings (CasP), yam peelings (YamP), coconut husk (CocH), corncobs (CorC) and cornhusk (CorH) generated at 600 °C for 2 h.

From Figure 5, the ashes of the untreated biomass fuels indicated the presence of black particles (fixed carbon). A plausible explanation for the formation of black particles, as explained by Krishnarao et al. [106], is that, during the combustion of biomass fuels

from room temperature to high temperature, there is a simultaneous decomposition and oxidation of the organic matter into carbon. Prior to the removal of all the carbon, if the temperature rise is higher than the melting temperature of potassium oxide (350 °C), surface melting or sintering of the ash occurs, and the K^+ ions trap the carbon inside the organic matrix. This phenomenon inhibits carbon removal and results in the formation of black particles at high temperatures [106–108]. This explains the basis for the higher LOI values (indirect carbon content) measured in the untreated samples compared to the acid-treated biomass samples. Since the potassium oxide concentration is higher in the untreated biomass fuels than the acid-treated biomass, there was a high propensity for black particles formation in the ashes [106].

Furthermore, chemical pre-treatment hydrolyses the organic (i.e., cellulose, hemicellulose and lignin) compounds and break their structures down [109–111]. Therefore, the evolution of volatile matter in the pre-treated samples could easily occur, decreasing the amount of residual carbon in ashes [112]. Comparatively, the ashes at 1 w/v% CA had few remnants of black particles than the ashes of 5 w/v% CA for the same reasons explained above. Analysis of the metallic impurities shown in Figure 4 confirms a higher concentration of K^+ ions in the 1 w/v% CA than the ashes of 5 w/v% CA. Hence, the tendency to form black particles was more pronounced than the ashes from 5 w/v% CA treated samples. Chakraverty et al. [113] obtained ash completely white in colour after leaching rice husk in dilute 1 N HCl, thus proving the effectiveness of acid pre-treatment in mitigating the formation of black particles. The complete white colour of CorC-A-5% and CorH-A-5% indicates total amorphous structured silica [114], as it is proven by the XRD measurements.

3.5.2. Nitrogen Gas Adsorption-Desorption Measurements

The isotherms for the CorH-U-A, CorH-A-1% and CorH-A-5% are given in Figure 6 as examples since the other samples show similar behaviour; the corresponding textural properties data along with the different samples are summarized in Table 4. For the treated samples (CorH-A-1% and CorH-A-5%), the isotherms exhibited a common characteristic of type IV(a) isotherm according to the IUPAC classifications [115], with a small knee at $p/p_0 = 0.05$. They showed an H3 apparent hysteresis loop with closure points around $p/p_0 = 0.40$, which is often associated with the effects of capillary condensation in non-uniform pore arrangements [116,117]. In addition, the presence of hysteresis loop in isotherms has been attributed to the presence of larger mesopores in the ash, which can only be accessed through the smaller mesopores [115]. Furthermore, the isotherms followed a similar path at the lower regions, and the amount of nitrogen adsorbed increases when approaching the saturation vapour pressure ($p/p_0 = 1$). The absence of an apparent plateau close to $p/p_0 = 1$ implies the presence of larger meso and macropores, which cannot be fully filled with the nitrogen condensate [47] and/or the presence of interstices between particles.

Conversely, the isotherm for the untreated ash sample (CorH-U-A) exhibited a much lower nitrogen adsorption capacity with no visible hysteresis loop, indicating no or much smaller porosity than the acid-leached ash samples. Agglomeration of ash particles has been reported to be accelerated by the presence of alkali metals [118], which were high in CorH-U-A according to the elemental analysis in Figure 4, resulting in diminished porosity [119]. CorH-U-A might contain some microporosity, which might have been formed by possible agglomeration of ash particles [35].

The textural properties, including the specific surface area (BET) and pore volume (NLDFT) from the nitrogen adsorption-desorption isotherms of the untreated and acid leached ashes are given in Table 4.

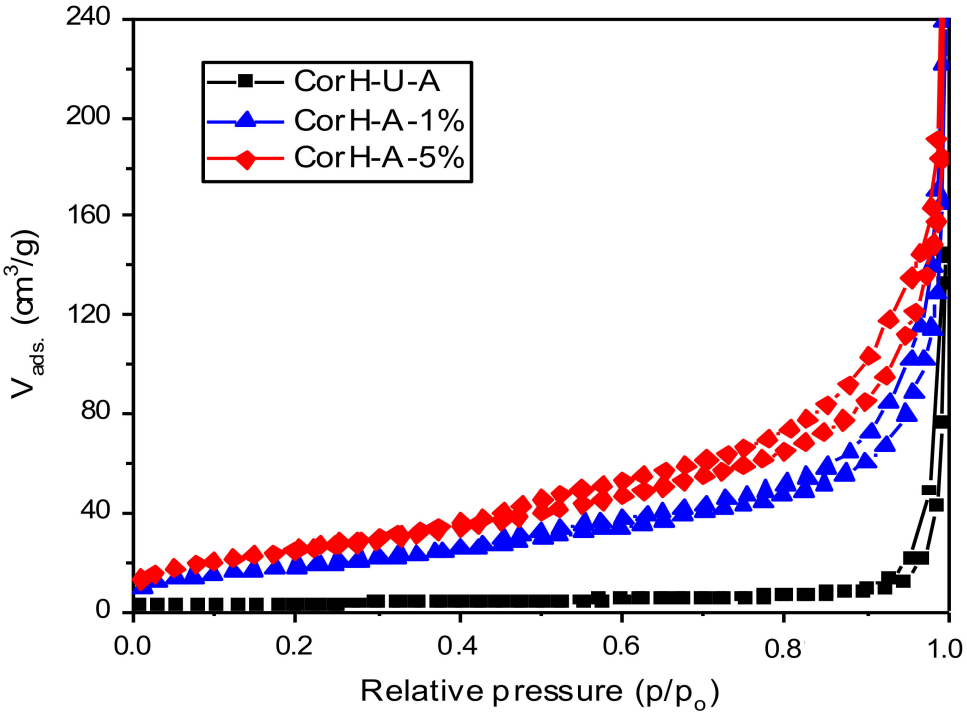

Figure 6. Adsorption–desorption isotherms of ashes from untreated and treated cornhusk.

Table 4. Comparison of the structural characteristics (S_{BET} and pore volume V_P) of ashes derived from biomass fuels leached in 1 *w*/*v*% CA and 5 *w*/*v*% CA at a combustion temperature of 600 °C and residence time of 2 h.

Sample	S_{BET} (m^2/g)	V_p (cm^3/g)
Untreated		
CasP-U-A	3	0
YamP-U-A	2	0
CocH-U-A	0	0
CorC-U-A	2	0.01
CorH-U-A	9	0.04
1 *w*/*v* % CA		
CasP-A-1%	16	0.06
YamP-A-1%	7	0.16
CocH-A-1%	20	0.05
CorC-A-1%	47	0.09
CorH-A-1%	67	0.17
5 *w*/*v* % CA		
CasP-A-5%	26	0.10
YamP-A-5%	5	0.02
CocH-A-5%	56	0.14
CorC-A-5%	70	0.14
CorH-A-5%	91	0.21

Ashes/biogenic silica from cassava and yam biomass fuels exhibited the lowest surface area and pore volume compared to those of the other biomass fuels. According to Soltani et al. [120], a chelate reaction occurs between the carboxyl group (-COOH) of the citric acid and the metal impurities in the biomass fuels. Consequently, hydrolysis of the organic matter cleaves the macromolecules (monosaccharides), thereby removing the embedded impurities and opening the pores within the biomass fuels [121]. Table 4 shows that the surface area and pore volume of the ashes (biogenic silica) increase with

increasing citric acid concentration for all biomass fuels investigated. For example, the specific area of the CorH-U-A was 9 m^2/g; however, after being treated with 1 w/v% citric acid, it increases to 67 m^2/g and continued up to 91 m^2/g at 5 w/v% CA concentration. Similarly, the pore volume of the ashes also increased in the order of preparation: X-A-5 w/v% > X-A-1 w/v% > X-U-A (X represents the name of the sample) within the different biogenic silica samples investigated.

The results obtained agree with similar observations made by Schneider et al. [47]. According to Schneider et al. [47], an increase in the purity of ashes (low presence of carbon and metallic impurities) will increase the surface areas and pore volumes due to pore blocking effects of the impurities present in the ashes. Hence, the purity of the ashes at 5 w/v% CA was higher than those of untreated and 1 w/v%. Moreover, a possible agglomeration of the ash particles of the untreated samples might have resulted in a diminished porosity [119]. It is conceivable that at 1 w/v% citric acid solution, the maximal removal capacity for metal impurities was achieved. Additional impurities could not be removed further to increase the pores/holes between the molecules. Secondly, these pores are developed within the particles by the thermal decomposition process. Since the carbon is easily volatized in the treated samples during combustion, the pore walls are disintegrated, resulting in a rise in mesopore volume [93,94]. In addition, the textural variation between the individual biomasses is most likely since distinct Si integration mechanisms and varying SiO_2 domains exist among the various plants and plant parts investigated [34].

3.5.3. Phase Analysis of the Biomass Ash Samples

Venezia et al. [122] reported that the presence of alkali ions such as K, Mg, and Na in the ashes results in low melting temperature alkali-rich compounds, which drives the transition to different crystalline phases of silica. In addition, Yang et al. [123] reported that these metallic species accelerate the crystallization of amorphous silica above 1000 °C. Thus, eutectic mixtures or silica phases are induced, decreasing the phase transition temperature from amorphous to crystalline silica. These minerals, introduced as fuel contaminants, result in a less active amorphous silica with low textural properties [115] due to the strong correlation between the crystallinity fraction and porosity changes of the silica-rich ashes [50]. This phenomenon is even more pronounced for untreated biomass fuels, as mentioned in the study of Schneider et al. [35,47] during their investigations with rice husk.

Figure 7 shows the XRD patterns and crystalline phases identified in the ash samples of the biomass fuels pre-treated with 1 w/v% citric acid. In all the ash samples, the following dominant phases were detected: quartz (SiO_2), calcite ($CaCO_3$) and anhydrite [$Ca(SO_4)$]. The presence of these dominant phases has also been reported during the investigations of wheat straw, miscanthus and cereal remnant pellet, all leached in hot solution of sulfuric acid [20]. Other minor crystalline phases, such as feldspar of the plagioclase series such as albite [$Na(AlSi_3O_8)$], were found in cassava and yam peelings as well as coconut husk in addition to an amorphous fraction. Potassium feldspar, such as sanidine ($KAlSi_3O_8$) was clearly detected in CocH-A-1%. The formation of sanidine ($KAlSi_3O_8$), as reported in the study of Alyosef et al. [20] could be as a result of a thermodynamic effect (i.e., "back-formation" of feldspar or arcanite) that reduces part of the amorphous silica particles [10,100]. The major differences in the XRD patterns of the samples were that of the CorC-A-1%, CorH-A-1%, which were characterized by a clear and dominant amorphous component with traces of arcanite (K_2SO_4) and anhydrite [$Ca(SO_4)$], respectively. These last two phases are because of the remaining low impurities of K_2O and CaO present in the ashes, as confirmed by the EDX spectrum of the CorH-A-1% sample in Figure 8.

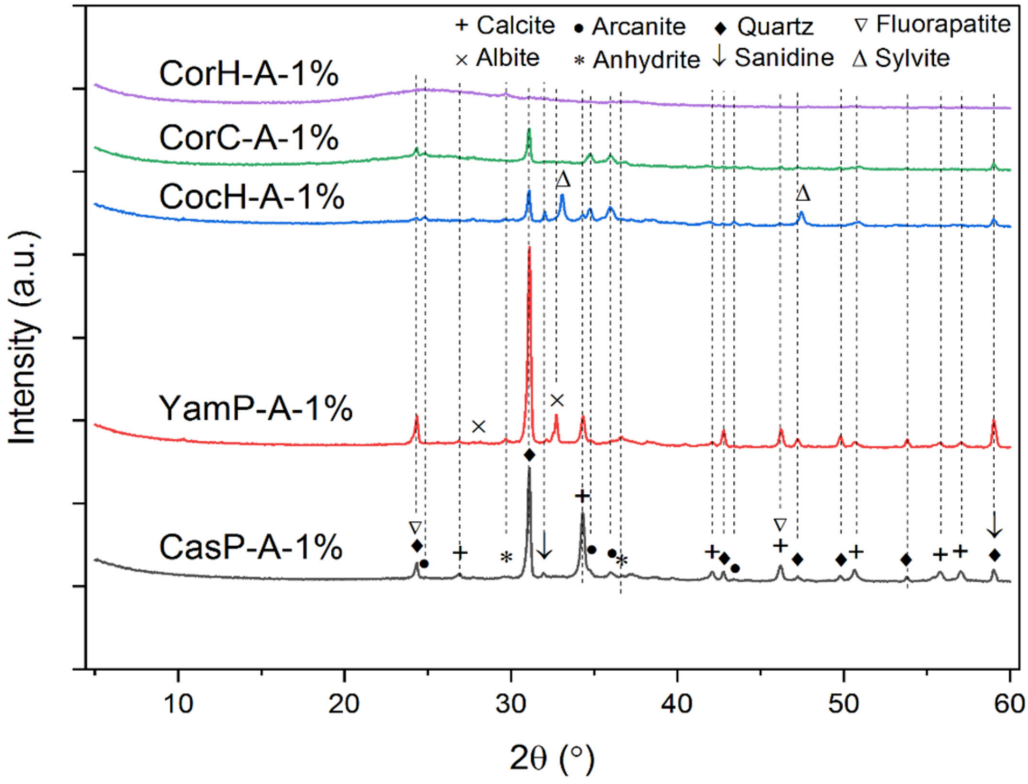

Figure 7. X-ray diffraction pattern of the ash samples resulting from the combustion of 1 w/v% acid-treated biomass fuels at 600 °C.

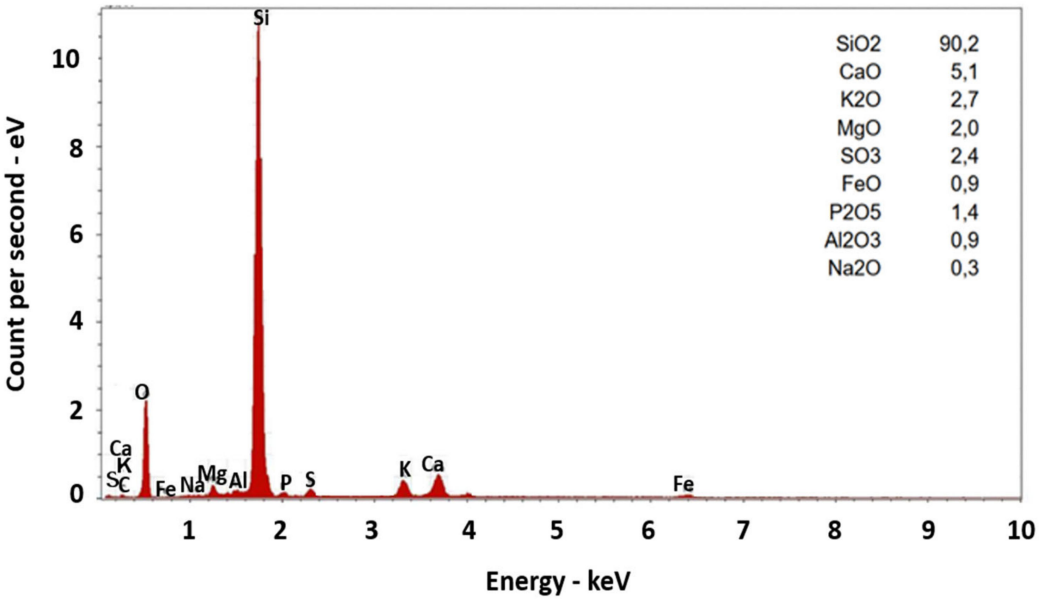

Figure 8. EDX spectrum (30 kV) of the ash sample (wt.% db = 100) resulting from the combustion of CorH-A-1%.

According to the literature, the phase formations in the ashes can be attributed to the high presence of critical ash forming elements (such as Ca, K and Na) and their interactions with the silica particles [50,124–126]. Comparing the elemental compositions of the ashes of the biomass fuels leached at 1 w/v% citric acid, all ash samples except for CorC-A-1% and CorH-A-1% had a higher content of potassium and sodium oxide (see "Elemental Composition of ashes in Figure 4). Thus, the tendencies for the formation of these minerals (fuel contaminants), i.e., anhydrite $Ca(SO_4)$, quartz (SiO_2), arcanite (K_2SO_4),

sylvite (KCl), calcite and albite [$Na(AlSi_3O_8)$] were more evident in those samples as confirmed by the XRD measurements and summarized in Table 5. The broad peak in the range of 2Theta = 20–30° found in the cornhusk ash samples was predominantly due to the amorphous silica in the analyzed samples in Figure 7. The thermally unstable phase of calcite ($CaCO_3$) was also observed in some of the samples, especially cassava and yam peels, and this was due to the high concentration of Ca^{2+} ions in the water used for the leaching. This observation is in line with the results from the FTIR analyses where bands of calcite were dominant. Deng et al. [127] also reported on the formation of calcite on –OH surfaces in high Ca^{2+} concentration.

Table 5. Crystalline phases identified with XRD in the ash samples after the combustion of 1 *w*/*v*% acid-treated biomass fuels at 600 °C.

	Ashes				
Phase	**CasP-A-1%**	**YamP-A-1%**	**CocH-A-1%**	**CorC-A-1%**	**CorH-A-1%**
Anhydrite [$Ca(SO_4)$]	x	x			x
Quartz (SiO_2)	x	x	x	x	x
Arcanite (K_2SO_4)	x		x		
Sylvite (KCl)			x		
Calcite ($CaCO_3$)	x	x	x		
Albite [$Na(AlSi_3O_8)$]		x			
Sanidine ($KAlSi_3O_8$)	x	x	x		

"x" denoting the presence of such a phase in the ashes.

A recent study of Beidaghy Dizaji et al. [50] on rice husk and straw ashes showed that once the temperature exceeds 550 towards 700 °C, there is a high tendency to form thermally non-stable compounds such as arcanite, calcite, and sylvite, which were also observed in this study. The result of this study only showed the presence of quartz instead of the other stable polymorphs forms of silica, i.e., cristobalite and tridymite [83,93,123]. The formation of cristobalite and tridymite phases in ashes is reported to occur at temperatures above 800 °C, lower than the temperature at which the selected biomass fuels in this study were combusted. Vassilev et al. [128] also reported the formation of cristobalite in rice husk ashes produced at higher temperatures (900 °C) as the main crystalline silica phase. The absence of cristobalite and tridymite in our ash samples affirms the appropriateness of the selected temperature regime for the combustion of the biomass fuels. This is because a high percentage of cristobalite and tridymite in ashes could negatively impact the textural properties and pose other health risks due to the carcinogenic attribute of crystalline silica [50,129].

Figure 9 also shows the improvement of silica content by employing higher citric acid concentration during the pre-treatment stage. As observed, the O-Si-O bands at CorH-A-5% are of higher intensity than those of CorH-A-1%. More importantly, they are comparable to the bands of commercial reference silica (CWK Köstropur® 021012) on the market, paving the way for the possibility of a wide variety of applications. The literature also reported silica purity improvement by pre-treatment of other silica-rich biomass fuels [20,125].

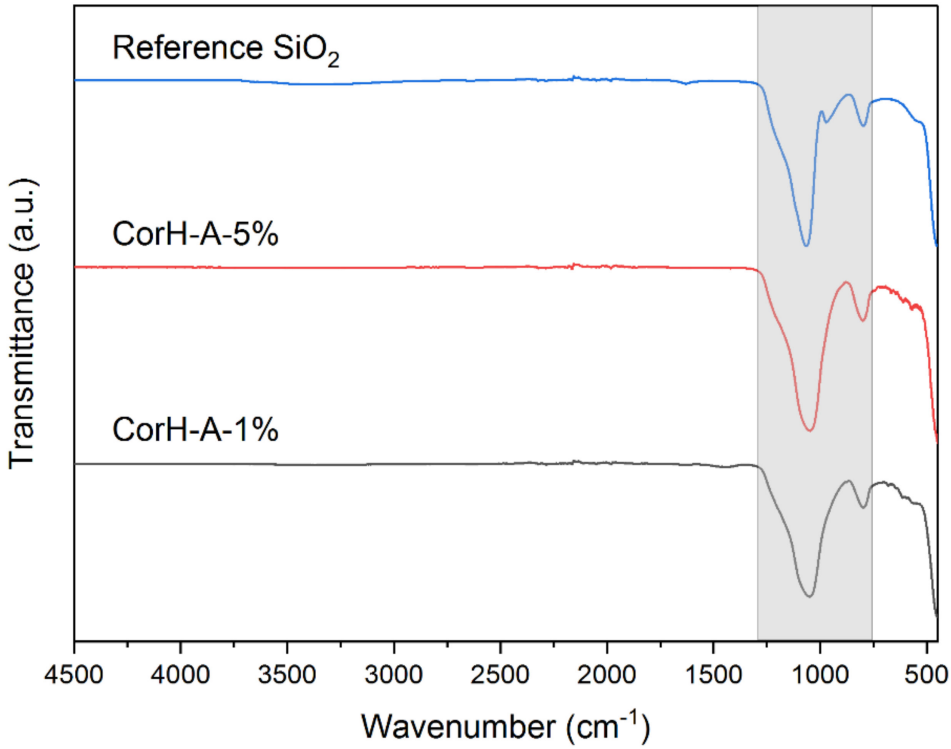

Figure 9. Comparison of the FTIR patterns of CorH-A-1% and CorH-A-5% with commercially available silica (CWK Köstropur® 021012) in the market (purity > 99.9%).

4. Conclusions

This work systematically examined the potential of producing high-quality amorphous silica from African biomass fuels such as cassava, yam, coconut, corncob, and cornhusk. The results showed that the leaching of the biomass fuels effectively removed a significant fraction of metallic impurities, especially K_2O and carbon compounds, from the organic matrix. The relative reductions of K_2O by the citric acid in yam peel was the lowest (79 wt.% db) in comparison to 92, 97, 98 and 97 wt.% db calculated for corncob, cassava peel, coconut husk and cornhusk, respectively. Acid leaching of the biomass in 5 w/v% citric acid resulted in producing ashes with larger surface areas, pore volume and completely white (no traces of carbon). The colour, surface area and pore volume of the resulting ashes after combustion were highly influenced by the initial composition of the biomass fuels and the concentration of citric acid used in the pre-treatment step. Cornhusk ash obtained the highest surface area (91 m^2/g) and the highest silica content (>90 wt.% db), which was completely amorphous along with corncob (85 wt.% db SiO_2). However, crystalline phases such as arcanite (K_2SO_4), sylvite (KCl) and calcite ($CaCO_3$) were found in the ashes of cassava, yam, and coconut due to the influence of potassium and calcium ions. Consequently, the existing pre-treatment and combustion methods should be optimized and extensively investigated to avoid phase formations. After these modifications, the production of biogenic silica products, which has already been realized in rice husk ash should be possible from cassava, yam, and coconut residues. The results of this study widen the fundamental knowledge for the preparation of value-added materials from primary but less-known African residues opening up new value chains for the recovery of silica from cassava, yam, coconut, corncob, and cornhusk.

Author Contributions: Conceptualization, C.O.P., S.F. and M.N.; methodology, C.O.P.; formal analysis, C.O.P.; investigation, C.O.P.; resources, C.O.P. and S.F.; data curation, C.O.P. and H.B.D.; writing—original draft preparation, C.O.P.; writing—review and editing, C.O.P., S.F., T.S. and H.B.D.; visualization, C.O.P., S.F., H.B.D. and T.S.; supervision, S.F. and M.N.; project administration, S.F. and M.N. All authors have read and agreed to the published version of the manuscript.

Funding: This research was funded by the Federal Ministry of Food and Agriculture (BMEL) under the Grant Number 2819DOKA05.

Institutional Review Board Statement: Not applicable.

Informed Consent Statement: Not applicable.

Data Availability Statement: Not applicable.

Acknowledgments: Special gratitude to the analytical laboratory and technical team members of DBFZ for their invaluable support during this study. Special appreciation to Marc Bohnet and Christoph Kröhl for their commitments to the analyses of the biomass fuels.

Conflicts of Interest: The authors declare no conflict of interest.

Abbreviations

The following abbreviations are used in the manuscript:

CasP	Cassava peelings
YamP	Yam peelings
CocH	Coconut husk
CorC	Corncob
CorH	Cornhusk
CasP-U	Untreated cassava peelings
YamP-U	Untreated yam peelings
CocH-U	Untreated coconut husk
CorC-U	Untreated cornhusk
CorH-U	Untreated cornhusk
YamP-1%	Yam peelings leached in 1 w/v% citric acid
CocH-1%	Coconut husk leached in 1 w/v% citric acid
CorC-1%	Corncob leached in 1 w/v% citric acid
CorH-1%	Cornhusk leached in 1 w/v% citric acid
CasP-U-A	Ash of untreated cassava peelings
YamP-U-A	Ash of untreated yam peelings
CocH-U-A	Ash of untreated coconut husk
CorC-U-A	Ash of untreated corncob
CorH-U-A	Ash of untreated cornhusk
CasP-A-1%	Ash of 1 w/v% acid-leached cassava peelings
YamP-A-1%	Ash of 1 w/v% acid-leached yam peelings
CocH-A-1%	Ash of 1 w/v% acid-leached coconut husk
CorC-A-1%	Ash of 1 w/v% acid-leached corncob
CorH-A-1%	Ash of 1 w/v% acid-leached cornhusk
CasP-A-5%	Ash of 5 w/v% acid-leached cassava peelings
YamP-A-5%	Ash of 5 w/v% acid-leached yam peelings
CocH-A-5%	Ash of 5 w/v% acid-leached coconut husk
CorC-A-5%	Ash of 5 w/v% acid-leached corncob
CorH-A-5%	Ash of 5 w/v% acid-leached cornhusk
VM	Volatile matter
AC	Ash content
MC	Moisture content
LHV	Lower heating value.
wb	Wet basis
wt.%	Weight percentage
db	Dry basis
n.d.	Not detected
CA	Citric acid

References

1. Shah, M.A.; Khan, M.N.S.; Kumar, V. Biomass residue characterization for their potential application as biofuels. *J. Therm. Anal. Calorim.* **2018**, *134*, 2137–2145. [CrossRef]
2. Jiang, L.; Hu, S.; Sun, L.-S.; Su, S.; Xu, K.; He, L.-M.; Xiang, J. Influence of different demineralization treatments on physicochemical structure and thermal degradation of biomass. *Bioresour. Technol.* **2013**, *146*, 254–260. [CrossRef]
3. Marland, G. Accounting for Carbon Dioxide Emissions from Bioenergy Systems. *J. Ind. Ecol.* **2010**, *14*, 866–869. [CrossRef]
4. Duku, M.H.; Gu, S.; Ben Hagan, E. A comprehensive review of biomass resources and biofuels potential in Ghana. *Renew. Sustain. Energy Rev.* **2011**, *15*, 404–415. [CrossRef]
5. Lim, J.S.; Manan, Z.A.; Alwi, S.R.W.; Hashim, H. A review on utilisation of biomass from rice industry as a source of renewable energy. *Renew. Sustain. Energy Rev.* **2012**, *16*, 3084–3094. [CrossRef]
6. Kemausuor, F.; Kamp, A.; Thomsen, S.T.; Bensah, E.; Østergård, H. Assessment of biomass residue availability and bioenergy yields in Ghana. *Resour. Conserv. Recycl.* **2014**, *86*, 28–37. [CrossRef]
7. United Nations Framework Convention on Climate Change. Adoption of the Paris Agreement: Proposal by the President. In Proceedings of the Paris Climate Change Conference, Paris, France, 30 November–12 December 2015.
8. African Climate Policy Centre (ACPC). 2010. Overview of the ClimDev Africa Programme. Available online: http://www.climdev-africa.org/afrian-climate-policy-center (accessed on 28 September 2021).
9. Catuti, M.; Elkerbout, M.; Alessi, M.; Egenhofer, C. Biomass and Climate Neutrality: CEPS Policy Insights. No 2020-19. August 2020. Available online: https://www.ceps.eu/wp-content/uploads/2020/08/PI2020-19_Biomass-and-climate-neutrality.pdf (accessed on 28 September 2021).
10. Guimarães, J.; Frollini, E.; da Silva, C.G.; Wypych, F.; Satyanarayana, K. Characterization of banana, sugarcane bagasse and sponge gourd fibers of Brazil. *Ind. Crop. Prod.* **2009**, *30*, 407–415. [CrossRef]
11. Milbrandt, A. *Assessment of Biomass Resources in Liberia*; No. NREL/TP-6A2-44808; National Renewable Energy Lab. (NREL): Golden, CO, USA, 2009.
12. Smith, O.B. Utilization of Crop Residues in the Nutrition of Sheep and Goats in the Humid Tropics of West Africa. In *Sheep and Goat Meat Production in Humid Tropics of West Africa*; FAO Animal Production and Health Paper; Atta Krah, A.N., Reyholds, L., Eds.; FAO: Rome, Italy, 1987; Available online: http://www.fao.org/library/library-home/en/ (accessed on 29 September 2021).
13. Abass, A.; Mlingi, N.; Ranaivoson, R.; Zulu, M.; Mukuka, I.; Abele, S.; Bachwenkizi, B.; Cromme, N. *Potential for Commercial Production and Marketing of Cassava: Experiences from the Small-Scale Cassava Processing Project in East and Southern Africa*; IITA: Ibadan, Nigeria, 2013.
14. Titiloye, J.; Abu Bakar, M.S.; Odetoye, T. Thermochemical characterisation of agricultural wastes from West Africa. *Ind. Crop. Prod.* **2013**, *47*, 199–203. [CrossRef]
15. Adepoju, A.D.; Adebisi, J.A.; Odusote, J.K.; Ahmed, I.I.; Hassan, S.B. Preparation of Silica from Cassava Periderm. *J. Solid Waste Technol. Manag.* **2016**, *42*, 216–221. [CrossRef]
16. Jekayinfa, S.O.; Scholz, V. Potential Availability of Energetically Usable Crop Residues in Nigeria. *Energy Sources Part A Recover. Util. Environ. Eff.* **2009**, *31*, 687–697. [CrossRef]
17. Cooper, C.; Laing, C. A macro analysis of crop residue and animal wastes as a potential energy source in Africa. *J. Energy S. Afr.* **2007**, *18*, 10–19. [CrossRef]
18. Dasappa, S. Potential of biomass energy for electricity generation in sub-Saharan Africa. *Energy Sustain. Dev.* **2011**, *15*, 203–213. [CrossRef]
19. Stecher, K.; Brosowski, A.; Thrän, D. Biomass Potential in Africa. Irena 2013. Available online: https://www.dbfz.de/fileadmin/user_upload/Referenzen/Broschueren/IRENA-DBFZ_Biomass_Potential_in_Africa.pdf (accessed on 4 October 2021).
20. Alyosef, H.A.; Schneider, D.; Wassersleben, S.; Roggendorf, H.; Weiß, M.; Eilert, A.; Denecke, R.; Hartmann, I.; Enke, D. Meso/Macroporous Silica from Miscanthus, Cereal Remnant Pellets, and Wheat Straw. *ACS Sustain. Chem. Eng.* **2015**, *3*, 2012–2021. [CrossRef]
21. Nitsch, J.; Krewitt, W.; Langniss, O. Renewable Energy in Europe. *Encycl. Energy* **2004**, *5*, 313–331. [CrossRef]
22. Adebisi, J.A.; Agunsoye, J.O.; Bello, S.A.; Kolawole, F.O.; Ramakokovhu, M.M.; Daramola, M.O.; Hassan, S.B. Extraction of Silica from Sugarcane Bagasse, Cassava Periderm and Maize Stalk: Proximate Analysis and Physico-Chemical Properties of Wastes. *Waste Biomass Valorization* **2017**, *10*, 617–629. [CrossRef]
23. Omohimi, C.I.; Piccirillo, C.; Roriz, M.; Ferraro, V.; Vasconcelos, M.W.; Sanni, L.; Tomlins, K.; Pintado, M.M.; Abayomi, L.A. Study of the proximate and mineral composition of different Nigerian yam chips, flakes and flours. *J. Food Sci. Technol.* **2017**, *55*, 42–51. [CrossRef]
24. FAOSTAT. *The State of Food and Agriculture*; Food and Agriculture Organisation of the UN: Rome, Italy, 2007; Available online: http://www.fao.org/3/a1200e/a1200e.pdf (accessed on 21 August 2021).
25. Bonfim, W.B.; de Paula, H.M. Characterization of different biomass ashes as supplementary cementitious material to produce coating mortar. *J. Clean. Prod.* **2021**, *291*, 125869. [CrossRef]
26. Andreola, F.; Martín, M.; Ferrari, A.; Lancellotti, I.; Bondioli, F.; Rincón, J.; Romero, M.; Barbieri, L. Technological properties of glass-ceramic tiles obtained using rice husk ash as silica precursor. *Ceram. Int.* **2013**, *39*, 5427–5435. [CrossRef]
27. Sae-Oui, P.; Rakdee, C.; Thanmathorn, P. Use of rice husk ash as filler in natural rubber vulcanizates: In comparison with other commercial fillers. *J. Appl. Polym. Sci.* **2002**, *83*, 2485–2493. [CrossRef]

28. Ajmal, M.; Rao, R.A.K.; Anwar, S.; Ahmad, J.; Ahmad, R. Adsorption studies on rice husk: Removal and recovery of Cd(II) from wastewater. *Bioresour. Technol.* **2003**, *86*, 147–149. [CrossRef]
29. Niculescu, V.-C.; Miricioiu, M.; Geana, E.-I.; Ionete, R.-E.; Paun, N.; Parvulescu, V. Silica Mesoporous Materials -an Efficient Sorbent for Wine Polyphenols Separation. *Rev. Chim.* **2019**, *70*, 1513–1517. [CrossRef]
30. Liu, D.; Seeburg, D.; Kreft, S.; Bindig, R.; Hartmann, I.; Schneider, D.; Enke, D.; Wohlrab, S. Rice Husk Derived Porous Silica as Support for Pd and CeO2 for Low Temperature Catalytic Methane Combustion. *Catalyst* **2019**, *9*, 26. [CrossRef]
31. Azadi, M.; Bahrololoom, M.E.; Heidari, F. Enhancing the mechanical properties of an epoxy coating with rice husk ash, a green product. *J. Coat. Technol. Res.* **2010**, *8*, 117–123. [CrossRef]
32. Dai, H.; Yang, J.; Ma, J.; Chen, F.; Fei, Z.; Zhong, M. A green process for the synthesis of controllable mesoporous silica materials. *Microporous Mesoporous Mater.* **2012**, *147*, 281–285. [CrossRef]
33. Adebisi, J.; Agunsoye, J.; Bello, S.; Ahmed, I.; Ojo, O.; Hassan, S. Potential of producing solar grade silicon nanoparticles from selected agro-wastes: A review. *Sol. Energy* **2017**, *142*, 68–86. [CrossRef]
34. Florek, J.; Guillet-Nicolas, R.; Kleitz, F. Ordered mesoporous silica: Synthesis and applications. In *Functional Materials*; Walter de Gruyter GmbH & Co KG: Berlin, Germany, 2014; pp. 61–100.
35. Schneider, D. Biogenic Silica from Regional Feedstocks—Sustainable Synthesis and Characterization. Ph.D. Thesis, Universität Leipzig, Leipzig, Germany, 2019.
36. Beidaghy Dizaji, H.; Zeng, T.; Hartmann, I.; Enke, D.; Schliermann, T.; Lenz, V.; Bidabadi, M. Generation of High Quality Biogenic Silica by Combustion of Rice Husk and Rice Straw Combined with Pre- and Post-Treatment Strategies—A Review. *Appl. Sci.* **2019**, *9*, 1083. [CrossRef]
37. Quispe, I.; Navia, R.; Kahhat, R. Energy potential from rice husk through direct combustion and fast pyrolysis: A review. *Waste Manag.* **2017**, *59*, 200–210. [CrossRef]
38. Biswas, B.; Pandey, N.; Bisht, Y.; Singh, R.; Kumar, J.; Bhaskar, T. Pyrolysis of agricultural biomass residues: Comparative study of corn cob, wheat straw, rice straw and rice husk. *Bioresour. Technol.* **2017**, *237*, 57–63. [CrossRef] [PubMed]
39. Zemnukhova, L.A.; Egorov, A.G.; Fedorishcheva, G.A.; Barinov, N.N.; Sokol'Nitskaya, T.A.; Botsul, A.I. Properties of amorphous silica produced from rice and oat processing waste. *Inorg. Mater.* **2006**, *42*, 24–29. [CrossRef]
40. Ma, J.F.; Yamaji, N. Silicon uptake and accumulation in higher plants. *Trends Plant Sci.* **2006**, *11*, 392–397. [CrossRef] [PubMed]
41. Yan, G.; Nikolic, M.; Ye, M.-J.; Xiao, Z.-X.; Liang, Y.-C. Silicon acquisition and accumulation in plant and its significance for agriculture. *J. Integr. Agric.* **2018**, *17*, 2138–2150. [CrossRef]
42. Vaibhav, V.; Vijayalakshmi, U.; Roopan, S.M. Agricultural waste as a source for the production of silica nanoparticles. *Spectrochim. Acta Part A Mol. Biomol. Spectrosc.* **2015**, *139*, 515–520. [CrossRef] [PubMed]
43. Abu Bakar, R.; Yahya, R.; Gan, S.N. Production of High Purity Amorphous Silica from Rice Husk. *Procedia Chem.* **2016**, *19*, 189–195. [CrossRef]
44. Miricioiu, M.G.; Niculescu, V.-C. Fly Ash, from Recycling to Potential Raw Material for Mesoporous Silica Synthesis. *Nanomaterials* **2020**, *10*, 474. [CrossRef] [PubMed]
45. Behrens, M.; Datye, A.K. *Catalysis for the Conversion of Biomass and Its Derivatives*; Max Planck Research Library for History and Development of Knowledge: Berlin, Germany, 2013.
46. Long, J.; Song, H.; Jun, X.; Sheng, S.; Lun-Shi, S.; Kai, X.; Yao, Y. Release characteristics of alkali and alkaline earth metallic species during biomass pyrolysis and steam gasification process. *Bioresour. Technol.* **2012**, *116*, 278–284. [CrossRef]
47. Schneider, D.; Wassersleben, S.; Weiß, M.; Denecke, R.; Stark, A.; Enke, D. A Generalized Procedure for the Production of High-Grade, Porous Biogenic Silica. *Waste Biomass Valorization* **2020**, *11*, 1–15. [CrossRef]
48. Umeda, J.; Imai, H.; Kondoh, K. Polysaccharide hydrolysis and metallic impurities removal behaviour of rice husks in citric aicd leaching treatment. *Trans. JWRI* **2009**, *38*, 13–18.
49. Umeda, J.; Kondoh, K. High-purity amorphous silica originated in rice husks via carboxylic acid leaching process. *J. Mater. Sci.* **2008**, *43*, 7084–7090. [CrossRef]
50. Beidaghy Dizaji, H.; Zeng, T.; Hölzig, H.; Bauer, J.; Klöß, G.; Enke, D. Ash transformation mechanism during combustion of rice husk and rice straw. *Fuel* **2022**, *307*, 121768. [CrossRef]
51. Utsev, J.T.; Taku, J.K. Coconut Shell Ash as Partial Replacement of Ordinary Portland Cement In Concrete Production. *Int. J. Sci. Technol. Res.* **2012**, *1*, 86–89.
52. Samanta, A.K.; Basu, G.; Mishra, L. Role of major constituents of coconut fibres on absorption of ionic dyes. *Ind. Crop. Prod.* **2018**, *117*, 20–27. [CrossRef]
53. Asuquo, E.D.; Martin, A.D.; Nzerem, P. Evaluation of Cd(II) Ion Removal from Aqueous Solution by a Low-Cost Adsorbent Prepared from White Yam (Dioscorea rotundata) Waste Using Batch Sorption. *ChemEngineering* **2018**, *2*, 35. [CrossRef]
54. Anuar, M.F.; Fen, Y.W.; Zaid, M.H.M.; Matori, K.A.; Khaidir, R.E.M. Synthesis and structural properties of coconut husk as potential silica source. *Results Phys.* **2018**, *11*, 1–4. [CrossRef]
55. Schliermann, T.; Hartmann, I.; Beidaghy Dizaji, H.; Zeng, T.; Schneider, D.; Wassersleben, S.; Enke, D.; Jobst, T.; Lange, A.; Roelofs, F.; et al. High Quality Biogenic Silica from Combined Energetic and Material Utilization of Agricultural Residues. In Proceedings of the 7th International Symposium on Energy from Biomass and Waste, Venice, Italy, 15–18 October 2018; ISBN 978-8-86-265013-7.
56. Hilbers, T.J.; Wang, Z.; Pecha, B.; Westerhof, R.J.; Kersten, S.R.; Pelaez-Samaniego, M.R.; Garcia-Perez, M. Cellulose-Lignin interactions during slow and fast pyrolysis. *J. Anal. Appl. Pyrolysis* **2015**, *114*, 197–207. [CrossRef]

57. Chen, D.; Gao, A.; Cen, K.; Zhang, J.; Cao, X.; Ma, Z. Investigation of biomass torrefaction based on three major components: Hemicellulose, cellulose, and lignin. *Energy Convers. Manag.* **2018**, *169*, 228–237. [CrossRef]
58. Ma, Z.; Chen, D.; Gu, J.; Bao, B.; Zhang, Q. Determination of pyrolysis characteristics and kinetics of palm kernel shell using TGA–FTIR and model-free integral methods. *Energy Convers. Manag.* **2015**, *89*, 251–259. [CrossRef]
59. Zhao, C.; Jiang, E.; Chen, A. Volatile production from pyrolysis of cellulose, hemicellulose and lignin. *J. Energy Inst.* **2017**, *90*, 902–913. [CrossRef]
60. Yang, H.; Yan, R.; Chen, H.; Lee, D.H.; Zheng, C. Characteristics of hemicellulose, cellulose and lignin pyrolysis. *Fuel* **2007**, *86*, 1781–1788. [CrossRef]
61. Dhyani, V.; Bhaskar, T. A comprehensive review on the pyrolysis of lignocellulosic biomass. *Renew. Energy* **2018**, *129*, 695–716. [CrossRef]
62. Lopez-Velazquez, M.A.; Santes, V.; Balmaseda, J.; Torres-Garcia, E. Pyrolysis of orange waste: A thermo-kinetic study. *J. Anal. Appl. Pyrolysis* **2013**, *99*, 170–177. [CrossRef]
63. Yang, H.; Yan, R.; Chin, T.; Liang, D.T.; Chen, A.H.; Zheng, C. Thermogravimetric Analysis−Fourier Transform Infrared Analysis of Palm Oil Waste Pyrolysis. *Energy Fuels* **2004**, *18*, 1814–1821. [CrossRef]
64. Mendes, C.A.; Adnet, F.A.; Leite, M.C.A.M.; Furtado, C.; Furtado, M. Chemical, physical, mechanical, thermal and morphological characterization of corn husk residue. *Cellul. Chem. Technol.* **2015**, *49*, 727–735.
65. Ceylan, S.; Topçu, Y. Pyrolysis kinetics of hazelnut husk using thermogravimetric analysis. *Bioresour. Technol.* **2014**, *156*, 182–188. [CrossRef] [PubMed]
66. Gu, X.; Ma, X.; Li, L.; Liu, C.; Cheng, K.; Li, Z. Pyrolysis of poplar wood sawdust by TG-FTIR and Py–GC/MS. *J. Anal. Appl. Pyrolysis* **2013**, *102*, 16–23. [CrossRef]
67. Jiang, Z.; Liu, Z.; Fei, B.; Cai, Z.; Yu, Y.; Liu, X. The pyrolysis characteristics of moso bamboo. *J. Anal. Appl. Pyrolysis* **2012**, *94*, 48–52. [CrossRef]
68. Kumar, A.; Wang, L.; Dzenis, Y.A.; Jones, D.D.; Hanna, M.A. Thermogravimetric characterization of corn stover as gasification and pyrolysis feedstock. *Biomass Bioenergy* **2008**, *32*, 460–467. [CrossRef]
69. Chen, D.; Zheng, Y.; Zhu, X. In-depth investigation on the pyrolysis kinetics of raw biomass. Part I: Kinetic analysis for the drying and devolatilization stages. *Bioresour. Technol.* **2013**, *131*, 40–46. [CrossRef] [PubMed]
70. Amutio, M.; Lopez, G.; Aguado, R.; Artetxe, M.; Bilbao, J.; Olazar, M. Kinetic study of lignocellulosic biomass oxidative pyrolysis. *Fuel* **2012**, *95*, 305–311. [CrossRef]
71. Mansaray, A.E.G.K.G. Kinetics of the Thermal Degradation of Rice Husks in Nitrogen Atmosphere. *Energy Sources* **1999**, *21*, 773–784. [CrossRef]
72. Jose, A.; Nivitha, M.; Krishnan, M.; Robinson, R. Characterization of cement stabilized pond ash using FTIR spectroscopy. *Constr. Build. Mater.* **2020**, *263*, 120136. [CrossRef]
73. Jung, H.; Kwak, H.; Chun, J.; Oh, K. Alkaline Fractionation and Subsequent Production of Nano-Structured Silica and Cellulose Nano-Fibrils for the Comprehensive Utilization of Rice Husk. *Sustainability* **2021**, *13*, 1951. [CrossRef]
74. Nakason, K.; Khemthong, P.; Kraithong, W.; Chukaew, P.; Panyapinyopol, B.; Kitkaew, D.; Pavasant, P. Upgrading properties of biochar fuel derived from cassava rhizome via torrefaction: Effect of sweeping gas atmospheres and its economic feasibility. *Case Stud. Therm. Eng.* **2021**, *23*, 100823. [CrossRef]
75. Pollard, Z.A.; Goldfarb, J.L. Valorization of cherry pits: Great Lakes agro-industrial waste to mediate Great Lakes water quality. *Environ. Pollut.* **2021**, *270*, 116073. [CrossRef]
76. Volpe, M.; Goldfarb, J.L.; Fiori, L. Hydrothermal carbonization of Opuntia ficus-indica cladodes: Role of process parameters on hydrochar properties. *Bioresour. Technol.* **2018**, *247*, 310–318. [CrossRef] [PubMed]
77. Magdziarz, A.; Dalai, A.K.; Koziński, J.A. Chemical composition, character and reactivity of renewable fuel ashes. *Fuel* **2016**, *176*, 135–145. [CrossRef]
78. Nieves, L.J.J.; Elyseu, F.; Goulart, S.; Pereira, M.D.S.; Valvassori, E.Z.; Bernardin, A.M. Use of fly and bottom ashes from a thermoelectrical plant in the synthesis of geopolymers: Evaluation of reaction efficiency. *Energy Geosci.* **2021**, *2*, 167–173. [CrossRef]
79. Nana, A.; Epey, N.; Rodrique, K.C.; Deutou, J.G.N.; Djobo, J.N.Y.; Tomé, S.; Alomayri, T.S.; Ngouné, J.; Kamseu, E.; Leonelli, C. Mechanical strength and microstructure of metakaolin/volcanic ash-based geopolymer composites reinforced with reactive silica from rice husk ash (RHA). *Materialia* **2021**, *16*, 101083. [CrossRef]
80. Ma, X.; Zhou, B.; Gao, W.; Qu, Y.; Wang, L.; Wang, Z.; Zhu, Y. A recyclable method for production of pure silica from rice hull ash. *Powder Technol.* **2012**, *217*, 497–501. [CrossRef]
81. Bathla, A.; Narula, C.; Chauhan, R.P. Hydrothermal synthesis and characterization of silica nanowires using rice husk ash: An agricultural waste. *J. Mater. Sci. Mater. Electron.* **2018**, *29*, 6225–6231. [CrossRef]
82. Morrow, B.A.; McFarlan, A.J. Surface vibrational modes of silanol groups on silica. *J. Phys. Chem.* **1992**, *96*, 1395–1400. [CrossRef]
83. Mohanraj, K.; Kannan, S.; Barathan, S.; Sivakumar, G. Preparation and Characterization of Nano SiO_2 from Corn Cob Ash by Precipitation Method. *Optoelectron. Adv. Mater. Rapid Commun.* **2012**, *6*, 394–397.
84. Ennaciri, Y.; El Alaoui-Belghiti, H.; Bettach, M. Comparative study of K2SO4 production by wet conversion from phosphogypsum and synthetic gypsum. *J. Mater. Res. Technol.* **2019**, *8*, 2586–2596. [CrossRef]

85. Medina, J.M.; Del Bosque, I.F.S.; Frías, M.; De Rojas, M.I.S.; Medina, C. Characterisation and valorisation of biomass waste as a possible addition in eco-cement design. *Mater. Struct.* **2017**, *50*, 207. [CrossRef]
86. Liou, T.-H. Evolution of chemistry and morphology during the carbonization and combustion of rice husk. *Carbon* **2004**, *42*, 785–794. [CrossRef]
87. Frías, M.; Villar-Cociña, E.; Savastano, H. Brazilian sugar cane bagasse ashes from the cogeneration industry as active pozzolans for cement manufacture. *Cem. Concr. Compos.* **2011**, *33*, 490–496. [CrossRef]
88. Leng, L.; Bogush, A.A.; Roy, A.; Stegemann, J.A. Characterisation of ashes from waste biomass power plants and phosphorus recovery. *Sci. Total Environ.* **2019**, *690*, 573–583. [CrossRef] [PubMed]
89. Alyosef, H.A.; Ibrahim, S.; Welscher, J.; Inayat, A.; Eilert, A.; Denecke, R.; Schwieger, W.; Münster, T.; Kloess, G.; Einicke, W.-D.; et al. Effect of acid treatment on the chemical composition and the structure of Egyptian diatomite. *Int. J. Miner. Process.* **2014**, *132*, 17–25. [CrossRef]
90. Keown, D.; Favas, G.; Hayashi, J.; Li, C.-Z. Volatilisation of alkali and alkaline earth metallic species during the pyrolysis of biomass: Differences between sugar cane bagasse and cane trash. *Bioresour. Technol.* **2005**, *96*, 1570–1577. [CrossRef] [PubMed]
91. Chen, H.; Wang, W.; Martin, J.C.; Oliphant, A.J.; Doerr, P.A.; Xu, J.F.; DeBorn, K.M.; Chen, C.; Sun, L. Extraction of Lignocellulose and Synthesis of Porous Silica Nanoparticles from Rice Husks: A Comprehensive Utilization of Rice Husk Biomass. *ACS Sustain. Chem. Eng.* **2012**, *1*, 254–259. [CrossRef]
92. Dunlop, A.P. Furfural Formation and Behavior. *Ind. Eng. Chem.* **1948**, *40*, 204–209. [CrossRef]
93. Olsson, J.G.; Jäglid, U.; Pettersson, J.B.C.; Hald, P. Alkali Metal Emission during Pyrolysis of Biomass. *Energy Fuels* **1997**, *11*, 779–784. [CrossRef]
94. Hunt, L.P.; Dismukes, J.P.; Amick, J.A.; Schei, A.; Larsen, K. Rice Hulls as a Raw Material for Producing Silicon. *J. Electrochem. Soc.* **1984**, *131*, 1683–1686. [CrossRef]
95. Amick, J.A. Purification of Rice Hulls as a Source of Solar Grade Silicon for Solar Cells. *J. Electrochem. Soc.* **1982**, *129*, 864–866. [CrossRef]
96. Umeda, J.; Katsuyoshi, K. Process Optimization to Prepare High-Purity Amorphous Silica from Rice Husks via Citric Acid Leaching Treatment. *Trans. JWRI* **2008**, *37*, 13–17.
97. Currie, H.A.; Perry, C.C. Silica in Plants: Biological, Biochemical and Chemical Studies. *Ann. Bot.* **2007**, *100*, 1383–1389. [CrossRef] [PubMed]
98. Ma, J.F.; Yamaji, N. Functions and transport of silicon in plants. *Cell. Mol. Life Sci.* **2008**, *65*, 3049–3057. [CrossRef]
99. Singh, S.P.; Endley, N. Fabrication of nano-silica from agricultural residue and their application. In *Nanomaterials for Agriculture and Forestry Applications*; Elsevier: Amsterdam, The Netherlands, 2020; pp. 107–134.
100. Alyosef, H.A.; Eilert, A.; Welscher, J.; Ibrahim, S.S.; Denecke, R.; Schwieger, W.; Enke, D. Characterization of Biogenic Silica Generated by Thermo Chemical Treatment of Rice Husk. *Part. Sci. Technol.* **2013**, *31*, 524–532. [CrossRef]
101. Chandrasekhar, S.; Satyanarayana, K.G.; Pramada, P.N.; Raghavan, P.; Gupta, T.N. Review Processing, properties and applications of reactive silica from rice husk—An overview. *J. Mater. Sci.* **2003**, *38*, 3159–3168. [CrossRef]
102. Ma, J.F.; Higashitani, A.; Sato, K.; Takeda, K. Genotypic variation in silicon concentration of barley grain. *Plant Soil* **2003**, *249*, 383–387. [CrossRef]
103. Takahashi, E.; Ma, J.F.; Miyake, Y. The Possibility of Silicon as an Essential Element for Higher Plants. *Comments Agric. Food Chem.* **1990**, *2*, 99–122.
104. Broadley, M.; Brown, P.; Cakmak, I.; Ma, J.F.; Rengel, Z.; Zhao, F. *Beneficial Elements*; Elsevier: Amsterdam, The Netherlands, 2012; pp. 249–269.
105. Deren, C. Chapter 8 Plant genotype, silicon concentration, and silicon-related responses. *Inulin Inulin-Contain. Crop.* **2001**, *8*, 149–158. [CrossRef]
106. Krishnarao, R.; Subrahmanyam, J.; Kumar, T.J. Studies on the formation of black particles in rice husk silica ash. *J. Eur. Ceram. Soc.* **2001**, *21*, 99–104. [CrossRef]
107. Zareihassangheshlaghi, A.; Beidaghy Dizaji, H.; Zeng, T.; Huth, P.; Ruf, T.; Denecke, R.; Enke, D. Behavior of Metal Impurities on Surface and Bulk of Biogenic Silica from Rice Husk Combustion and the Impact on Ash-Melting Tendency. *ACS Sustain. Chem. Eng.* **2020**, *8*, 10369–10379. [CrossRef]
108. Chandrasekhar, S.; Pramada, P.N.; Majeed, J. Effect of calcination temperature and heating rate on the optical properties and reactivity of rice husk ash. *J. Mater. Sci.* **2006**, *41*, 7926–7933. [CrossRef]
109. Kumar, P.; Barrett, D.M.; Delwiche, M.J.; Stroeve, P. Methods for Pre-treatment of Lignocellulosic Biomass for Efficient Hydrolysis and Biofuel Production. *Ind. Eng. Chem. Res.* **2009**, *48*, 3713–3729. [CrossRef]
110. Mosier, N.; Wyman, C.; Dale, B.; Elander, R.; Lee, Y.Y.; Holtzapple, M.; Ladisch, M. Features of promising technologies for pre-treatment of lignocellulosic biomass. *Bioresour. Technol.* **2005**, *96*, 673–686. [CrossRef] [PubMed]
111. Tadesse, H.; Luque, R. Advances on biomass pre-treatment using ionic liquids: An overview. *Energy Environ. Sci.* **2011**, *4*, 3913–3929. [CrossRef]
112. Hanna, S.; Farag, L.; Mansour, N. Pyrolysis and combustion of treated and untreated rice hulls. *Thermochim. Acta* **1984**, *81*, 77–86. [CrossRef]
113. Chakraverty, A.; Mishra, P.; Banerjee, H.D. Investigation of combustion of raw and acid-leached rice husk for production of pure amorphous white silica. *J. Mater. Sci.* **1988**, *23*, 21–24. [CrossRef]

114. Shen, Y.; Zhao, P.; Shao, Q. Porous silica and carbon derived materials from rice husk pyrolysis char. *Microporous Mesoporous Mater.* **2014**, *188*, 46–76. [CrossRef]
115. Thommes, M.; Kaneko, K.; Neimark, A.V.; Olivier, J.P.; Rodriguez-Reinoso, F.; Rouquerol, J.; Sing, K.S.W. Physisorption of gases, with special reference to the evaluation of surface area and pore size distribution (IUPAC Technical Report). *Pure Appl. Chem.* **2015**, *87*, 1051–1069. [CrossRef]
116. Banerjee, S.; Gautam, R.K.; Jaiswal, A.; Chattopadhyaya, M.C.; Sharma, Y.C. Rapid scavenging of methylene blue dye from a liquid phase by adsorption on alumina nanoparticles. *RSC Adv.* **2015**, *5*, 14425–14440. [CrossRef]
117. Li, T.; Shen, J.; Huang, S.; Li, N.; Ye, M. Hydrothermal carbonization synthesis of a novel montmorillonite supported carbon nanosphere adsorbent for removal of Cr (VI) from waste water. *Appl. Clay Sci.* **2014**, *93–94*, 48–55. [CrossRef]
118. Basu, P. Biomass Characteristics. In *Biomass Gasification, Pyrolysis and Torrefaction*; Elsevier: Amsterdam, The Netherlands, 2018; pp. 49–91.
119. Shen, J.; Liu, X.; Zhu, S.; Zhang, H.; Tan, J. Effects of calcination parameters on the silica phase of original and leached rice husk ash. *Mater. Lett.* **2011**, *65*, 1179–1183. [CrossRef]
120. Soltani, N.; Bahrami, A.; Pech-Canul, M.; González, L. Review on the physicochemical treatments of rice husk for production of advanced materials. *Chem. Eng. J.* **2015**, *264*, 899–935. [CrossRef]
121. Ozdemir, S.; Ozdemir, S.; Yetilmezsoy, K. Poultry abattoir sludge as bio-nutrient source for walnut plantation in low-fertility soil. *Environ. Prog. Sustain. Energy* **2019**, *38*, e13066. [CrossRef]
122. Venezia, A.M.; La Parola, V.; Longo, A.; Martorana, A. Effect of Alkali Ions on the Amorphous to Crystalline Phase Transition of Silica. *J. Solid State Chem.* **2001**, *161*, 373–378. [CrossRef]
123. Yang, H.; Liu, B.; Chen, Y.; Li, B.; Chen, H. Influence of Inherent Silicon and Metals in Rice Husk on the Char Properties and Associated Silica Structure. *Energy Fuels* **2015**, *29*, 7327–7334. [CrossRef]
124. Gilbe, C.; Öhman, M.; Lindström, E.; Boström, D.; Backman, R.; Samuelsson, R.; Burvall, J. Slagging Characteristics during Residential Combustion of Biomass Pellets. *Energy Fuels* **2008**, *22*, 3536–3543. [CrossRef]
125. Strandberg, A.; Skoglund, N.; Thyrel, M.; Lestander, T.A.; Broström, M.; Backman, R. Time-Resolved Study of Silicate Slag Formation During Combustion of Wheat Straw Pellets. *Energy Fuels* **2019**, *33*, 2308–2318. [CrossRef]
126. Boström, D.; Skoglund, N.; Grimm, A.; Boman, C.; Öhman, M.; Broström, M.; Backman, R. Ash Transformation Chemistry during Combustion of Biomass. *Energy Fuels* **2012**, *26*, 85–93. [CrossRef]
127. Deng, H.; Wang, X.-M.; Du, C.; Shen, X.-C.; Cui, F.-Z. Combined effect of ion concentration and functional groups on surface chemistry modulated CaCO3 crystallization. *CrystEngComm* **2012**, *14*, 6647–6653. [CrossRef]
128. Vassilev, S.V.; Baxter, D.; Vassileva, C.G. An overview of the behaviour of biomass during combustion: Part II. Ash fusion and ash formation mechanisms of biomass types. *Fuel* **2014**, *117*, 152–183. [CrossRef]
129. World Health Organization. Agents Classified by the IARC Monographs, World Health Organization. International Agency for Research on Cancer. 2016. Available online: https://monographs.iarc.who.int/agents-classified-by-the-iarc/ (accessed on 28 October 2021).